BOREAS An international journal of Quaternary research

Chronology and stratigraphy of the Magdalen Islands archipelago from the last glaciation to the early Holocene: new insights into the glacial and sea-level history of eastern Canada

AUDREY M. RÉMILLARD, GUILLAUME ST-ONGE, PASCAL BERNATCHEZ, BERNARD HÉTU, JAN-PIETER BUYLAERT, ANDREW S. MURRAY AND BENOIT VIGNEAULT

BOREAS

Rémillard, A. M., St-Onge, G., Bernatchez, P., Hétu, B., Buylaert, J.-P., Murray, A. S. & Vigneault, B.: Chronology and stratigraphy of the Magdalen Islands archipelago from the last glaciation to the early Holocene: new insights into the glacial and sea-level history of eastern Canada. *Boreas.* 10.1111/bor.12179. ISSN 0300-9483.

The Magdalen Islands (Québec, Canada) are a key location for unravelling the glacial and sea-level history of the Maritime Provinces of eastern Canada. Although many sedimentary sequences have been described in the literature, absolute ages are lacking, impeding an accurate interpretation of the deposits and the establishment of a precise chronological framework. This study provides a detailed description of 21 stratigraphical sequences located throughout the archipelago, as well as the first comprehensive luminescence chronology from the Last Glacial Maximum (LGM) to *c.* 10 ka. In addition to the five samples collected for age control purposes, 34 luminescence samples were taken from 17 different sites in glacial, periglacial and coastal deposits. The stratigraphical and chronological data reveal that the islands were at the crossroads of two icecaps during the LGM; the southern islands were glaciated by the Escuminac icecap located in the western Gulf of St. Lawrence whereas the northern archipelago was glaciated at the end of the LGM by an ice flow from Newfoundland. The glacial deposit covering the northern Magdalen Islands was associated with the Newfoundland icecap; here it is named the Grande-Entrée till and is dated to *c.* 20 ka. OSL ages between *c.* 23 and 17 ka acquired from cryopediment and coastal deposits on the southern islands indicate that this part of the archipelago was deglaciated shortly after the LGM and was affected by a high sea level and periglacial processes. Around 15 ka, the entire archipelago was deglaciated and partially submerged until *c.* 10 ka. This data set is the first major contribution to a detailed chronology of the Magdalen Islands and constitutes the first step towards interpreting the glacial and sea-level history of the central area of the Gulf of St. Lawrence; this new understanding will provide input to regional marine and glacial modelling.

Audrey M. Rémillard (audrey.mercierremillard@uqar.ca) and Guillaume St-Onge, Institut des sciences de la mer de Rimouski (ISMER) & GEOTOP, Université du Québec à Rimouski, 310 allée des Ursulines, Rimouski, QC G5L 3A1, Canada; Pascal Bernatchez and Bernard Hétu, Département de biologie, chimie et géographie & Centre for Northern Studies (CEN), Université du Québec à Rimouski, 300 allée des Ursulines, Rimouski, QC, G5L 3A1, Canada; Jan-Pieter Buylaert and Andrew S. Murray, Nordic Laboratory for Luminescence Dating, Department of Geoscience, Aarhus University, Risø Campus, DK-4000 Roskilde, Denmark; Jan-Pieter Buylaert, Centre for Nuclear Technologies, Technical University of Denmark, Risø Campus, DK-4000 Roskilde, Denmark; Benoit Vigneault, Ministère du Développement durable, Environnement et Lutte contre les changements climatiques, 675 boul. René-Lévesque Est, Québec, QC G1R 5V7, Canada; *received 3rd August 2015, accepted 18th February 2016.*

The glacial history of the Maritime Provinces of eastern Canada has been debated throughout the 20th century. Two schools of thoughts have developed concerning the nature of the last glaciation in the area and these have become known as the 'maximum' and the 'minimum' conceptual models (e.g. Grant 1989; Stea *et al.* 1998, 2011). These models either argued that the Laurentide Ice Sheet (LIS) entirely covered the Maritimes to the end of the continental shelf (e.g. Dyke *et al.* 2002), or that local independent glaciers were located mainly on land with ice margins ending just offshore (e.g. Dyke & Prest 1987). The question of whether the Magdalen Islands, located in the centre of the Gulf of St. Lawrence (Fig. 1), were glaciated during the Last Glacial Maximum (LGM) is key to resolving this debate (e.g. Grant 1989). Several studies have focused on the palaeogeographical history of the islands but these have only served to strengthen the dispute between the maximum and minimum models, because some of these studies recognized evidence of glaciation, either from local glaciers or the LIS, whereas others argued that, during the last glaciation, the archipelago was ice-free (e.g. Richardson 1881; Chalmers 1895; Clarke 1911; Goldthwait 1915; Coleman 1919; Alcock 1941; Hamelin 1959; Prest *et al.* 1976; Dredge & Grant 1987; Parent & Dubois 1988; Dredge *et al.* 1992). More recently, regional syntheses have come to what is generally accepted in the literature as the Appalachian Glacier Complex (AGC; e.g. Stea *et al.* 1998, 2011; Josenhans & Lehman 1999; Stea 2004; Shaw *et al.* 2006; Josenhans 2007). The AGC suggests that local glaciers, mostly located on the Maritime Provinces, were coalescing with each other and with the LIS that formed an ice stream in the Laurentian Channel. This model results in a complex sea-level history in the Gulf of St. Lawrence that is variable both regionally and locally (e.g. Quinlan & Beaumont 1981; Shaw *et al.* 2002; Bell *et al.* 2005). Although the AGC is generally accepted, this conceptual model extrapolates from several studies under-

DOI 10.1111/bor.12179

taken throughout the Maritimes; little is actually known of the glacial history in the centre of the Gulf. Glacial, periglacial and marine deposits have been described in the literature (e.g. Prest *et al.* 1976; Dredge *et al.* 1992; Paquet 1989; Vigneault 2012; Rémillard *et al.* 2013, 2015a), but the Quaternary history of the islands remains poorly understood mostly because of the lack of a robust chronological framework. Nevertheless the archipelago offers a strategic terrestrial record; it is likely to have experienced and recorded the last glaciation(s) and the inherent sea-level and periglacial changes in a key area.

The oldest known record on the Magdalen Islands is located on Havre-Aubert Island and corresponds to a lagoonal marine deposit covering a woody peat. The wood provided U/Th Marine Isotopic Stage (MIS) 5 ages of 106.4±8.2 ka (UQT – 183), 101.7±15.6 ka (UQT – 182) and 89±7.6 ka (UQT – 184). The woody peat and the lagoon deposit are overlain by a littoral sandy and gravel ridge formed in a context of sea-level rise, which has itself been truncated by a local till associated with the MIS 4 (Dredge *et al.* 1992). More recently, based on a limited number of radiocarbon ages, Rémillard *et al.* (2013, 2015a) suggested that the southern part of the Magdalen Islands was glaciated by the Escuminac icecap that flowed towards the southeast at some point during MIS 2, and was affected by two marine transgressions and two periglacial phases both before and after the MIS 2 glaciation. Unfortunately, a similar chronological framework is lacking for other areas; the deposits of the archipelago require the construction of an absolute chronology before an understanding of the relationships amongst the glacial, periglacial and marine phases can be developed.

In this study, we aimed to (i) describe and characterize the sedimentology of 21 outcrops observed throughout the Magdalen Islands, (ii) improve the chronological framework by adding new OSL ages, and (iii) increase the understanding of the palaeogeography and sea-level history of a key area of eastern Canada, from the LGM to *c.* 10 ka.

Geological and geomorphological settings

The Magdalen Islands lie in the shallow waters of the Magdalen Shelf (<100 m) near the centre of the Gulf of St. Lawrence (47°N) (Fig. 1). Six of the seven islands are connected to each other by Holocene barrier beaches (tombolos) (Rémillard *et al.* 2015b). The islands are built on Carboniferous–Visean volcanic and sedimentary substrata (Brisebois 1981; Giles 2008). The geomorphology of the islands is dominated by basaltic conical hills surrounded by sandstone and shale platforms slightly inclined towards the sea, which are interpreted as cryopediment surfaces (Laverdière & Guimont 1974; Paquet 1989). The sandstone is mainly composed of quartz and is generally porous and highly friable (Brisebois 1981). On the southern islands, the bedrock is overlain discontinuously by between 0.5 and 10 m thick Quaternary sediments (e.g. Dredge *et al.* 1992; Rémillard *et al.* 2013). In the northern part of the archipelago (the Pointe-aux-Loups and Grande-Entrée Islands), sedimentary bodies can be ~20 m thick (e.g. Dredge *et al.* 1992; Vigneault 2012).

Methods

Sites

A total of 21 sedimentary outcrops mainly located in coastal cliffs have been described in detail (Fig. 1). Seven are located in the northern part of the Magdalen Islands (Old-Harry, Sandcove–Seacow, Bassin-aux-Huîtres west and east, Bluff-east, Pointe-aux-Loups north and south), two on Havre-aux-Maisons Island (Airport and HAM), seven on Cap-aux-Meules Island (Fatima, Facterie, SAQ, Arsène, Grader, Galet-Plat and Gros-Cap) and five on Havre-Aubert Island (ACW, AC-Lighthouse, AP-DEM, AP-CAM and Clermont). Finally, two sites were studied for chronological control purposes only: Plaisance, located on the tombolo connecting Cap-aux-Meules and Havre-Aubert Islands, and ACE, located on the southwest coast of Havre-Aubert Island.

Sedimentological analyses

Ten clast fabrics (n = 30, 49 or 50) were measured in the field using A-axis with an axial ratio of >1.5; eight of these were re-analysed from the study of Vigneault (2012). Clast fabrics were all plotted as contoured equal-area stereonets on the lower hemispheres using Stereo32 software and examined using eigenvector analysis (Mark 1973) (Table 1). Grain-size distribution of matrices was determined with a Beckman-Coulter particle size analyser LS 13 320 (0.04–2000 μm) on 51 disaggregated samples and processed with Gradistat v. 8.0 software using the logarithmic method of Folk & Ward (1957) (Blott & Pye 2001; Table S1). Altitudes were measured *in situ* using a Trimble RTK D-GPS (±0.015 m vertical uncertainty).

Radiocarbon dating

Samples of organic material were collected at the AC-Lighthouse and Clermont sites, both located on Havre-Aubert Island. The samples were prepared for radiocarbon dating at the radiochronology laboratory of Université Laval and analysed at the Keck Carbon Cycle AMS Facility at the University of California in Irvine. The conventional ^{14}C ages were calibrated using the CALIB 7.1 program with the INTCAL13 calibration data set (Reimer *et al.* 2013).

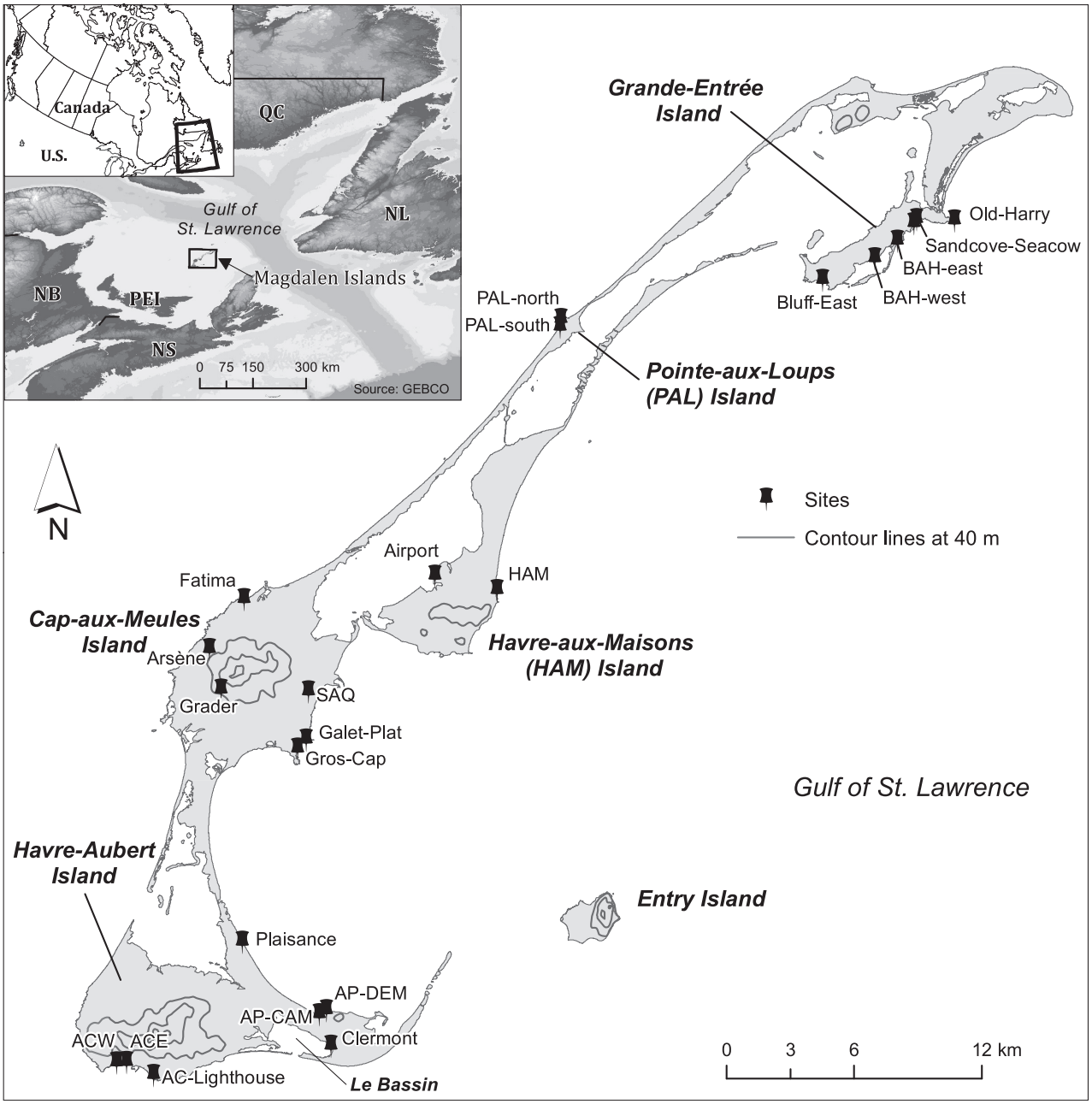

Fig. 1. Location of the Magdalen Islands in eastern Canada and the Gulf of St. Lawrence. Sample sites are shown as black pushpins.

Optically-Stimulated Luminescence (OSL) dating

Sampling, sample preparation and measurement protocols. – Thirty-nine OSL samples were collected throughout the archipelago from 19 sites (Tables 2, S2). Generally, sediments were sampled by hammering opaque plastic cylinders of 5 cm diameter and 30 cm in length into a homogeneous part of the deposit. For the pebbly units where the absence of sandy lenses did not allow this approach, samples were collected in the dark (at night) in opaque plastic bags (OSL80, OSL81, OSL83, OSL84 and OSL92). All samples were prepared under subdued orange light. The outer ~5 cm ends of the cylinder samples were used for water-content determination and dose-rate analysis. Samples were wet-sieved and the 180–250 μm (90–180 μm fraction for OSL08) fraction was etched with 10% HCl, 10% H_2O_2 and 10% HF in the usual manner. Heavy liquid separation (2.58 g ml^{-1}) was then used to separate quartz from K-rich feldspar grains. Finally, the quartz-rich extract was etched using concentrated HF (40%) for 1 h to remove any remaining

Table 1. Clast fabric data from this study. S = eigenvalues; K = shape parameter; C = strength parameter.

	Clast fabric ID	n	Mean vectors		Eigenvalues				
			Azimuth	Plunge	S1	S2	S3	K	C
PAL-North	CF01	49	96	26	0.622	0.246	0.132	1.496	1.546
PAL-South	CF02	50	77	20	0.558	0.322	0.120	0.560	1.537
Old-Harry	CF03	50	194	13	0.675	0.253	0.071	0.773	2.248
Old-Harry	CF04	50	21	2	0.705	0.186	0.109	2.499	1.865
BAH-West	CF05	50	61	28	0.618	0.256	0.127	1.251	1.585
BAH-East	CF06	49	87	20	0.663	0.215	0.123	2.016	1.688
BAH-East	CF07	50	49	37	0.735	0.160	0.105	3.642	1.946
Grader	CF08	50	22	14	0.635	0.285	0.080	0.634	2.071
Grader	CF09	49	15	9	0.764	0.182	0.055	1.195	2.636
Gros-Cap	CF10	30	54	12	0.665	0.236	0.099	1.197	1.902

feldspar and the outer alpha-irradiated layer from the quartz grains.

All measurements were carried out using Risø TL/OSL readers (model DA-20) each equipped with blue LEDs (470 nm, ~80 mW cm^{-2}), infrared (IR) LEDs (870 nm, ~135 mW cm^{-2}) and with a calibrated $^{90}Sr/^{90}Y$ beta source (Bøtter-Jensen *et al.* 2010). Quartz OSL was detected through a 7.5-mm Schott U-340 (UV) filter. The quartz extracts were mounted on ~8-mm-diameter stainless steel discs using 'Silkospray' silicone oil as a fixing agent. A single-aliquot regenerative-dose (SAR) protocol (Murray & Wintle 2000, 2003) was used for all equivalent dose (D_e) determinations. Prior to OSL measurement, the purity of the quartz extracts was confirmed by an OSL IR depletion test (Duller 2003); all samples had OSL IR depletion ratios within 10% of unity, indicating that there was no significant contribution from feldspar or other IR-sensitive components to the blue-stimulated OSL signals. Quartz aliquots were stimulated at 125 °C using blue light (90% power) for 40 s. Quartz D_e values were calculated using the first 0.32 s of the signal and a background based on the following 0.32–0.64 s to minimize any possible contribution of non-fast components (Cunningham & Wallinga 2010). The sample D_e used for the final age determination corresponds to the unweighted average of all accepted aliquots (between 21 and 48 aliquots per sample). As part of the investigation of the reliability of the quartz OSL ages, the feldspar extracts were also measured using infrared stimulation at elevated temperature and a SAR protocol. Details of these measurements are given in Appendix S1.

Radionuclide analysis and dosimetry. – Approximately 250–300 g of material was dried, ground and ignited (24 h at 450 °C) and subsequently cast in wax in a fixed cup-shaped geometry. After 3 weeks of storage to let ^{222}Rn reach equilibrium with its parent ^{226}Ra, the cups were counted on a high-resolution gamma spectrometer for at least 24 h following Murray *et al.* (1987). The radionuclide activities, water contents, dry dose rates and total dose rates are given in Table S2. Unfortunately, the ^{238}U concentrations are not known with sufficient precision to allow a discussion of the state of equilibrium between ^{226}Ra and ^{238}U on a sample-by-sample basis. However, it is interesting to note that the average $^{226}Ra/^{238}U$ ratio for all samples is 0.81 ± 0.09 (n = 39), suggesting that there may be some systematic disequilibrium in these samples. The most obvious explanation for a lack of ^{226}Ra in this environment is mobilization due to the high salinity at the time of deposition (Webster *et al.* 1995). Although most of these samples were collected from above sea level it is speculated that the considerable accumulation of salt spray on the islands and subsequent down washing by rain water is sufficient to continually remove some of the ^{226}Ra, maintaining this small disequilibrium. However, for these samples the U-series only contribute ~8% to the total dose rate and so a small U-series disequilibrium is not of significance. Dry dose rates were calculated from the radionuclide concentrations using the conversion factors given in Guérin *et al.* (2011). Field water contents were measured when the samples were first opened in the laboratory. Unfortunately, material was insufficient for saturation water content measurements on 14 out of the 39 samples. To overcome this problem, we used the saturation water content mean value of the other 25 available samples (numbers in italics in Table S2). Many of these samples were deposited under water but were, compared with their subsequent burial time, uplifted shortly after deposition. Other samples were deposited sub-aerially. All were subsequently well drained, and so for all samples (except the modern analogues), a lifetime water content of 50% of the saturation value was assumed with an absolute uncertainty of ±6%, e.g. for a sample with a saturation water content of 40% we adopted a lifetime average water content of 20±6%. For the three modern analogues where the likely fraction of saturation could be estimated more accurately, we adopted full saturation for sample OSL78 (subtidal) and 20% of saturation for samples OSL87 and OSL88 (beach). These assumed lifetime water contents were used to correct the calculated dry dose rates as described by Aitken (1985). Finally a cosmic ray dose rate was

Table 2. Sample location, elevation, depth, equivalent doses (D_e) and resulting quartz OSL ages. The index number column refers to Fig. 13. The equivalent dose tabulated is the average of 'n' estimates (total of 798 accepted estimates out of 802 measured aliquots). Samples in italic were saturated. The minimum dose is based on $2\times D_0$. The reliability of the quartz OSL ages is discussed in the *Reliability of the OSL ages* section.

Site	Sample ID	Environment	Index no.	Lat. (N)	Long. (W)	Elev. (m a.s.l.)	Depth (cm)	D_e (Gy)	Total dose rate (Gy ka^{-1})	n	Age±1σ (ka)	Well bleached?	
												Confident	Highly probable
ACE	OSL03	Beach	–	47.219517	61.989829	14.8	480	47±3	1.16±0.06	24	41±4		
ACE	OSL04	Beach	–	47.219517	61.989829	15.6	400	55±3	1.27±0.07	27	44±4		
ACW	OSL06	Subtidal	1	47.219500	61.995980	24	70	23.1±0.5	1.99±0.11	27	11.6±0.7	X	X
AC - Light	OSL08	Subtidal	–	47.213810	61.972999	12	300	83±5	2.18±0.12	30	38±3		X
AC - Light	OSL12	Subtidal	2	47.213810	61.972999	13	100	21.6±0.5	2.13±0.12	21	9.8±0.6	X	X
AP-DEM	OSL16	Subtidal	3	47.240281	61.865154	13.5	150	19.6±0.9	1.76±0.09	26	11.1±0.8	X	X
AP-DEM	OSL17	Subtidal	4	47.240281	61.865154	14.5	75	21.3±1.2	1.82±0.10	23	11.7±0.9	X	X
AP-CAM	OSL18	Subtidal	5	47.238646	61.869752	13	150	23.8±1.4	1.37±0.07	21	17.4±1.4	X	X
AP-CAM	OSL19	Subtidal	6	47.238646	61.869752	12.5	125	31.7±1.8	1.76±0.09	21	18.0±1.4		X
Bluff-east	OSL20	Marine	–	47.545753	61.548475	3	700	*>230*	1.54±0.09	–	>150	–	–
Bluff-east	OSL22	Marine	–	47.545753	61.548475	11	150	*>230*	1.99±0.10	–	>115	–	–
Bluff-east	OSL23	Subtidal	7	47.545753	61.548475	16	75	29.8±1.1	1.98±0.11	33	15.1±1.1	X	X
Sandcove	OSL26	Marine	–	47.568937	61.490783	6	1000	*>230*	1.47±0.08	–	>150	–	–
Sandcove	OSL29	Marine	–	47.568937	61.490783	15	100	*>230*	1.41±0.08	–	>156	–	–
Seacow	OSL30	Marine	–	47.570720	61.488940	10.5	300	*>230*	2.09±0.12	–	>110	–	–
Seacow	OSL31	Subtidal	8	47.570720	61.488940	11	250	21.7±1.0	1.71±0.10	32	12.6±1.0		X
Seacow	OSL32	Subtidal	9	47.570720	61.488940	12	150	17.5±0.7	1.55±0.08	21	11.3±0.8	X	X
Seacow	OSL33	Subtidal	10	47.570720	61.488940	13	50	14.7±0.5	1.45±0.08	21	10.1±0.6	X	X
PAL-north	OSL34	Marine	–	47.531185	61.712313	18	100	*>230*	1.77±0.10	–	>130	–	–
PAL-north	OSL36	Marine	–	47.531185	61.712313	8	1300	*>230*	1.45±0.09	–	>159	–	–
Airport	OSL44	Subtidal	11	47.423373	61.793613	2	175	14.9±0.7	1.31±0.07	33	11.4±0.9	X	X
Airport	OSL46	Subtidal	12	47.423373	61.793613	3	75	12.7±0.4	1.15±0.06	21	11.0±0.7	X	X
Fatima	OSL47	Subtidal	13	47.414613	61.912695	4.5	250	36.3±1.8	1.6±0.2	28	23±3	X	X
Fatima	OSL48	Subtidal	14	47.414613	61.912695	6	100	22.7±0.8	1.53±0.08	21	14.8±1.0	X	X
HAM	OSL63	Subtidal	15	47.416967	61.755060	9	90	31.6±1.3	1.37±0.07	21	23.0±1.6	X	X
Sandcove	OSL72	Subtidal	16	47.568937	61.490783	15.5	100	17.1±0.8	1.40±0.07	24	12.2±0.9	X	X
Airport	OSL78	Subtidal	–	47.423373	61.793613	−0.3	50	0.14±0.02	1.03±0.05	23	0.14±0.02		X
BAH-east	OSL79	Subtidal	17	47.561772	61.501402	4	100	17.4±0.8	1.60±0.05	24	10.9±0.8	X	X
Galet-Plat	OSL80	Beach	18	47.354933	61.875255	5.5	50	66±3	3.7±0.2	28	17.9±1.4		X
Galet-Plat	OSL81	Beach	19	47.354785	61.873007	4	50	81±4	3.8±0.2	23	21.1±1.7	X	X
SAQ	OSL83	Colluvial	–	47.375198	61.873500	10	75	45±3	3.04±0.17	22	14.9±1.2		X
Grader	OSL84	Colluvial	–	47.376529	61.927917	50	275	67±5	3.8±0.2	32	17.6±1.6	X	X
Plaisance	OSL87	Beach (dune)	–	47.269720	61.916940	4.8	10	0.08±0.05	1.57±0.09	48	0.05±0.03	X	X
Plaisance	OSL88	Beach (tidal)	–	47.269720	61.916940	0.5	20	0.10±0.07	1.91±0.11	24	0.05±0.04	X	X
Old-Harry	OSL89	Marine	–	47.569836	61.465471	11	300	*>230*	1.32±0.07	–	>174	–	–
Old-Harry	OSL90	Glacial	–	47.569836	61.465471	12.5	150	31.7±1.3	1.60±0.09	28	19.8±1.4		
Arsène	OSL92	Colluvial	–	47.393770	61.934643	50	50	51±2	2.61±0.15	26	19.5±1.4	X	X
PAL-north	OSL96	Subtidal	20	47.531185	61.712313	15.5	350	25.8±1.3	1.77±0.10	21	14.5±1.1		X
PAL-north	OSL97	Subtidal	21	47.531185	61.712313	18	100	21.3±0.8	1.66±0.09	24	12.8±0.9	X	X

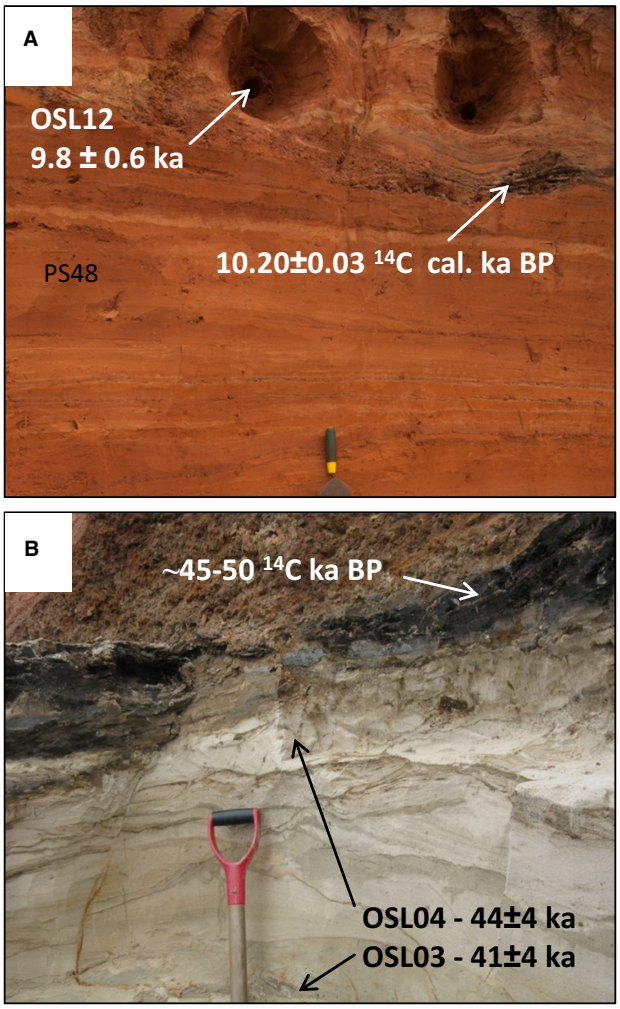

Fig. 2. Comparison of luminescence ages with radiocarbon ages for age control. A. The AC-Lighthouse site; OSL12 is compared with a new calibrated AMS ^{14}C age obtained on plant fragments. B. OSL03 and OSL04 are compared with radiocarbon ages already published in Rémillard *et al.* (2013).

estimated from the assumed lifetime burial depth, following the equations given by Prescott & Hutton (1994).

Age control. – In order to test the degree of bleaching of the coastal deposits, three samples of recently deposited coastal environments were collected as described above at two different sites: OSL78 from a subtidal environment (Airport site) and OSL87 and OSL88 from a beach (Plaisance site; Table 2). At two sites (ACE and AC-Lighthouse), luminescence ages are also compared with published radiocarbon ages and one new AMS ^{14}C age obtained on plant fragments (Fig. 2, Table 3). Note that the ACE site is not presented in the *Results and interpretations* section because the exposure has already been described and discussed in Rémillard *et al.* (2013); it is used here only for chronological control purposes.

Quartz luminescence characteristics. – Figure 3A illustrates a typical sensitivity-corrected growth curve with a natural OSL stimulation decay curve (inset), together with a decay curve from a quartz calibration standard (Hansen *et al.* 2015). The reproducibility of laboratory measurements using this material is illustrated by the two measurements of the sensitivity-corrected signal at 26 Gy. The average of this recycling ratio for all available measurements is 1.079±0.015 (n = 588). The growth curve also passes very close to the origin; the average recuperation is 0.09±0.08% of the natural signal (n = 588). The D_0 for this aliquot (Fig. 3A) is 115±14 Gy, suggesting that we can use this material to estimate D_e smaller than ~230 Gy (Wintle & Murray 2006).

The dependency of the D_e and the dose recovery ratio (Murray & Wintle 2003) on thermal pretreatment for sample OSL03 was tested by varying the preheat temperature; the thermal pretreatment employed after giving the test dose (the 'cut-heat') was 40 °C below the preheat temperature (except for 160 and 180 °C preheat for which the cut-heat was kept fixed at 160 °C; Fig. 3B, C). Both D_e estimates and dose recovery ratios have a pronounced dependence on preheat temperature with the dose recovery ratio only consistent with unity for preheats ≤220 °C (Fig. 3C). The D_e values are also relatively insensitive to preheat temperatures <220 °C. Because of this, we chose a preheat/cut-heat combination of 200/160 °C. Further dose recovery measurements (Murray & Wintle 2003) were made using six aliquots of all samples (except OSL80, OSL83, OSL88 and OSL97 because of lack of material) and given doses varying between 4 and 100 Gy

Table 3. List of radiocarbon ages discussed in this paper.

Site	Laboratory ID	Age (^{14}C a BP±1σ)	Calibrated age (±2σ)	Reference
ACE	UCIAMS-74416	>46 000	n/a	Rémillard *et al.* (2013)
ACE	UCIAMS-41189	47 100±2700	n/a	Rémillard *et al.* (2013)
ACE	UCIAMS-74417	50 100±3300	n/a	Rémillard *et al.* (2013)
ACE	UCIAMS-84792	47 100±2300	n/a	Rémillard *et al.* (2013)
ACE	UCIAMS-84793	47 800±2500	n/a	Rémillard *et al.* (2013)
AC-Lighthouse	UCIAMS-134737	8995±25	10 197±32	This paper
Clermont	UCIAMS-134729	9430±25	10 656±73	This paper

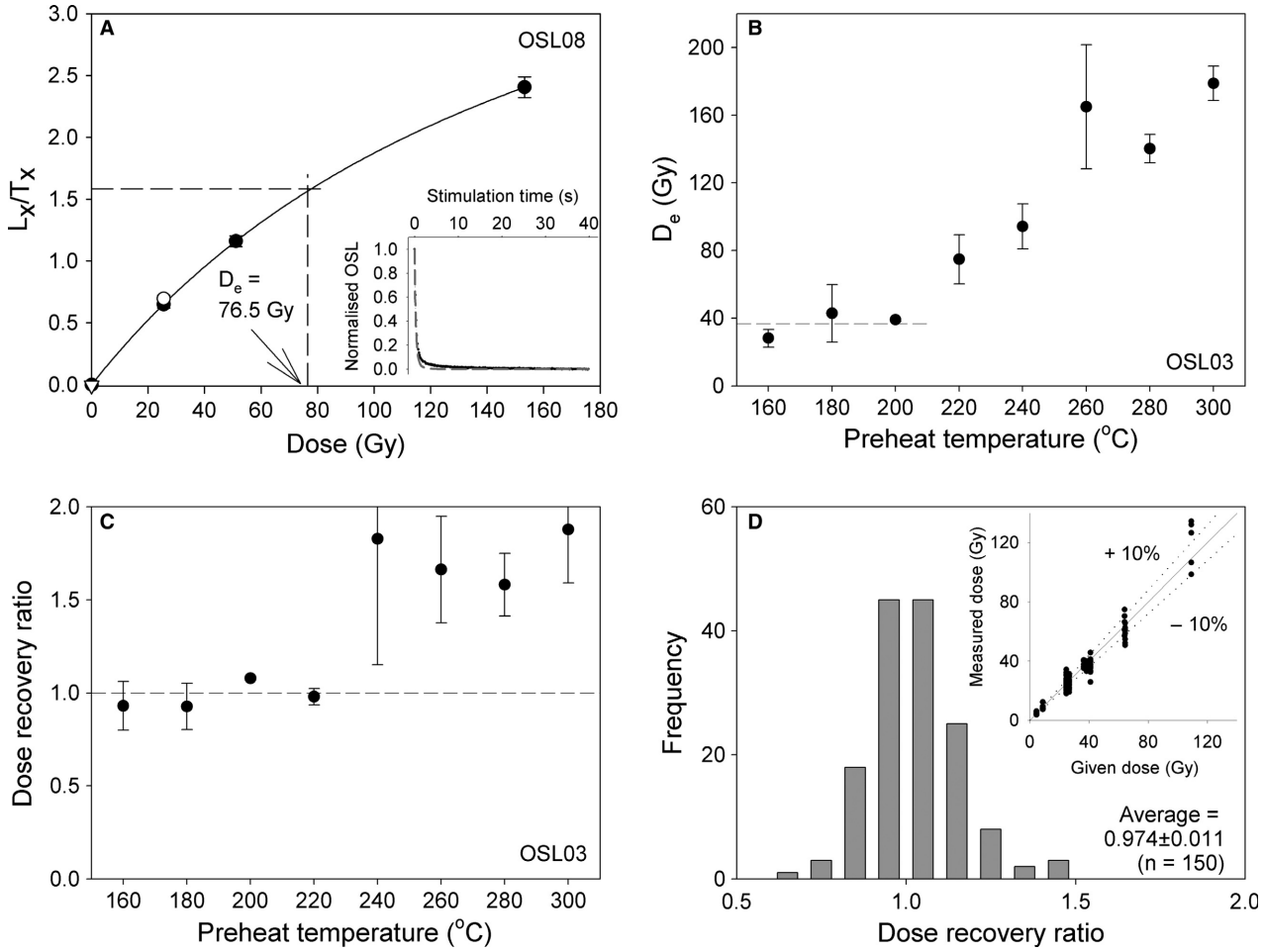

Fig. 3. A. Quartz OSL SAR growth curve from OSL08 (site AC-Lighthouse). Sensitivity-corrected regenerated signals are shown as filled circles, the unfilled circle represents a repeat point (recycling) and the open triangle the response to zero dose (recuperation). The sensitivity-corrected natural OSL signal is interpolated onto the growth curve to give the equivalent dose, D_e (in this case, 76.5 Gy). Inset shows a typical natural OSL decay from the same sample together with a decay curve of an aliquot of calibration quartz (dashed); a background signal from the end of the stimulation curve was subtracted before normalization. B. Preheat plateau test carried out on sample OSL03; each point represents the average of three aliquots. The dashed line represents the average D_e over the temperature range 160–200 °C. C. Dose recovery plateau test carried out on sample OSL03; each point represents the average of six aliquots. The dashed line represents a dose recovery ratio of unity. D. Summary of dose recovery data for all aliquots (n = 150) of 25 samples measured with a preheat of 200 °C for 10 s and cut-heat of 160 °C. Inset shows the measured doses plotted against the given doses.

depending on the approximate D_e of each sample (Fig. 3D); the average dose recovery ratio is 0.974±0.011 (n = 150), confirming that the chosen SAR protocol is suitable for these samples.

Reliability of the OSL ages. – Quartz from the Canadian Shield in mainland Quebec is not usually considered suitable for luminescence dating because of the low yield of sensitive grains (M. Lamothe, pers. comm. 2015). However, the sediment on and around the Magdalen Islands is not derived from the Canadian Shield, but rather from a Carboniferous sandstone platform derived from aeolian and fluvial sand (Brisebois 1981). This appears to have resulted in local quartz-rich sediment for which the OSL signal is dominated by a fast-component (e.g. Fig. 3A). The resulting OSL signals have satisfactory luminescence characteristics and the dose recovery ratios are indistinguishable from unity (Fig. 3).

Three samples were taken to represent modern analogues of the various coastal and subtidal deposits: OSL78 from a subtidal lagoon deposited in ~50 cm of water at low tide; OSL88 taken from just below the high tide limit on a beach, but deposited underwater; OSL87, aeolian sediment from an incipient dune just above the high tide limit. Samples OSL87 and OSL88 both give ages indistinguishable from zero (30±30 and 50±40 a) and even the subtidal lagoonal sediment has an apparent age of only 160±20 a. These quartz ages are very small compared with all those in Table 2, indicating that all the coastal/subtidal samples can probably be considered as well bleached. The limited independent age control can also be used to discuss the

completeness of bleaching of some of the samples at the time of deposition. OSL12 has a quartz OSL age of 9.8±0.6 ka and this sample sits immediately above a radiocarbon sample of 10.20±0.03 cal. ka BP (Fig. 2A). Figure 2B shows the stratigraphical relationship between five radiocarbon ages lying between 46 and 50 ka (Rémillard *et al.* 2013) and the chronostratigraphically consistent samples OSL03 (41±3 ka) and OSL04 (43±3 ka). The agreement between these OSL ages and the independent age control in both of these groups strongly suggests that the quartz OSL signal in all three of these subtidal/beach OSL samples was well bleached at the time of deposition. Furthermore, samples collected in a single unit are almost always consistent with each other (e.g. OSL03 and OSL04; OSL31, OSL32 and OSL33; OSL44 and OSL46; Table 2). The only exceptions are OSL08 and OSL12, which were sampled at the top and the base of a single unit and give ages of 38±3 and 9.8±0.6 ka, respectively. For safety reasons (very steep cliff), this outcrop was sampled at two different sections, one at the top and one at the base of the unit; it was not possible to completely connect these two sections stratigraphically. Thus it now seems likely that the sections were misidentified in the field, and that this explains the apparent stratigraphical inconsistency.

Further evidence for the completeness of bleaching of the quartz OSL signal at deposition is given by comparing the results with the less-bleachable K-feldspar (post-IR) IRSL signals (Murray *et al.* 2012; Buylaert *et al.* 2013) (analytical data and summary of feldspar results are given in Appendix S1). Feldspar IRSL signals are significantly more difficult to bleach than the OSL fast-component signal from quartz used here (Godfrey-Smith *et al.* 1988; Thomsen *et al.* 2008; Fig. S2). This provides an independent test of the degree of bleaching of our quartz. In Fig. S3 we compare the ages derived from the more difficult to bleach feldspar signals with those from quartz. As discussed in the Appendix S1, the feldspar data generally confirm the conclusion that our samples are well bleached, although there remain four samples for which, based only on feldspar, we cannot be confident of the completeness of bleaching of the quartz OSL signal prior to deposition. Amongst them, the two samples with the largest IR_{50} age overestimate compared to quartz (Fig. S3C) are OSL03 and OSL04; both of these samples have quartz D_e of <60 Gy and so are well below the ~230 Gy dating limit. Fortunately, OSL03 and OSL04 are the two samples for which we have independent age control based on radiocarbon (Fig. 2B); the agreement between the radiocarbon and quartz OSL ages clearly indicates that the quartz OSL signal from both these samples must have been sufficiently bleached at deposition. This calibrates our IR_{50} signal for use in testing quartz bleaching.

In summary, the agreement of the quartz OSL ages with modern analogues and radiocarbon age control, the internal consistency and the comparison with differential bleaching rates of IR_{50} and $pIRIR_{150}$ signals allows us to conclude that all the samples in this data set were very probably well bleached at deposition and are thus reliable.

Results and interpretations

Pointe-aux-Loups (PAL) north and south

Pointe-aux-Loups (PAL) Island is located on the northwest side of the Magdalen Islands (Fig. 1). On the western coast of the island, two active cliffs were described on each side of the wharf: PAL-north and PAL-south.

Sediments of the PAL-north exposure are ~18 m thick and ~60 m wide, filling a bedrock depression (Fig. 4A). The first unit (U1) lies directly on the sandstone bedrock and is composed of imbricated well-rounded pebbles and boulders, alternating with sand and gravel beds slightly inclined (~3–4°) southwards (Fig. 4B). These abrupt grain-size variations in U1 reflect several energy changes during deposition with periods of very high energy; some boulders reach more than a metre in diameter. A petrographic count (n = 100) carried out in U1 revealed that 66% of the pebbles and boulders are fossiliferous limestone from Anticosti Island located in the north of the Gulf of St. Lawrence, and 30% correspond to the St. Lawrence River North Shore geology (gneiss, granite, metaquartzite, anorthosite) (Vigneault 2012). With the exception of a few sandstone pebbles, the composition of U1 is entirely erratic. U1 evolves gradually into a stratified deposit (U2) composed of centimetric sandy beds alternating with millimetric silty beds inclined generally towards the southwest (Fig. 4C, D; Table S1); inclination of the beds increases from the base (~3–4°) to the top (>10°) (Vigneault 2012). U2 also contains scattered dropstones, which decrease in number from the base to the top. The top of U2 is characterized by many load structures (balls and pillows, flames) and deformations (faults and folds) (Fig. 4E). The quartz in U2 is completely saturated and so only a minimum age of >130 ka can be derived based on the $2\times D_0$ value >230 Gy (OSL34 and OSL36; Table 2). The entire U1 and U2 sequence is truncated by a compact and poorly sorted diamict (U3; Table S1) that appears either as a stone line or as remnant pockets. Figure 4E shows a remnant pocket in which clast fabric measurements suggest an E–W axis (inset Fig. 4E; Table 1). Some pebbles from U3 are striated and have contoured shapes. A petrographic count (n = 50) reveals that the unit is mostly erratic, composed of 80% metaquartzite, gabbro, schist and anorthosite, and 14% typical Appalachian lithology (jasper, phyllite, chert) (Vigneault 2012). U3 is overlaid

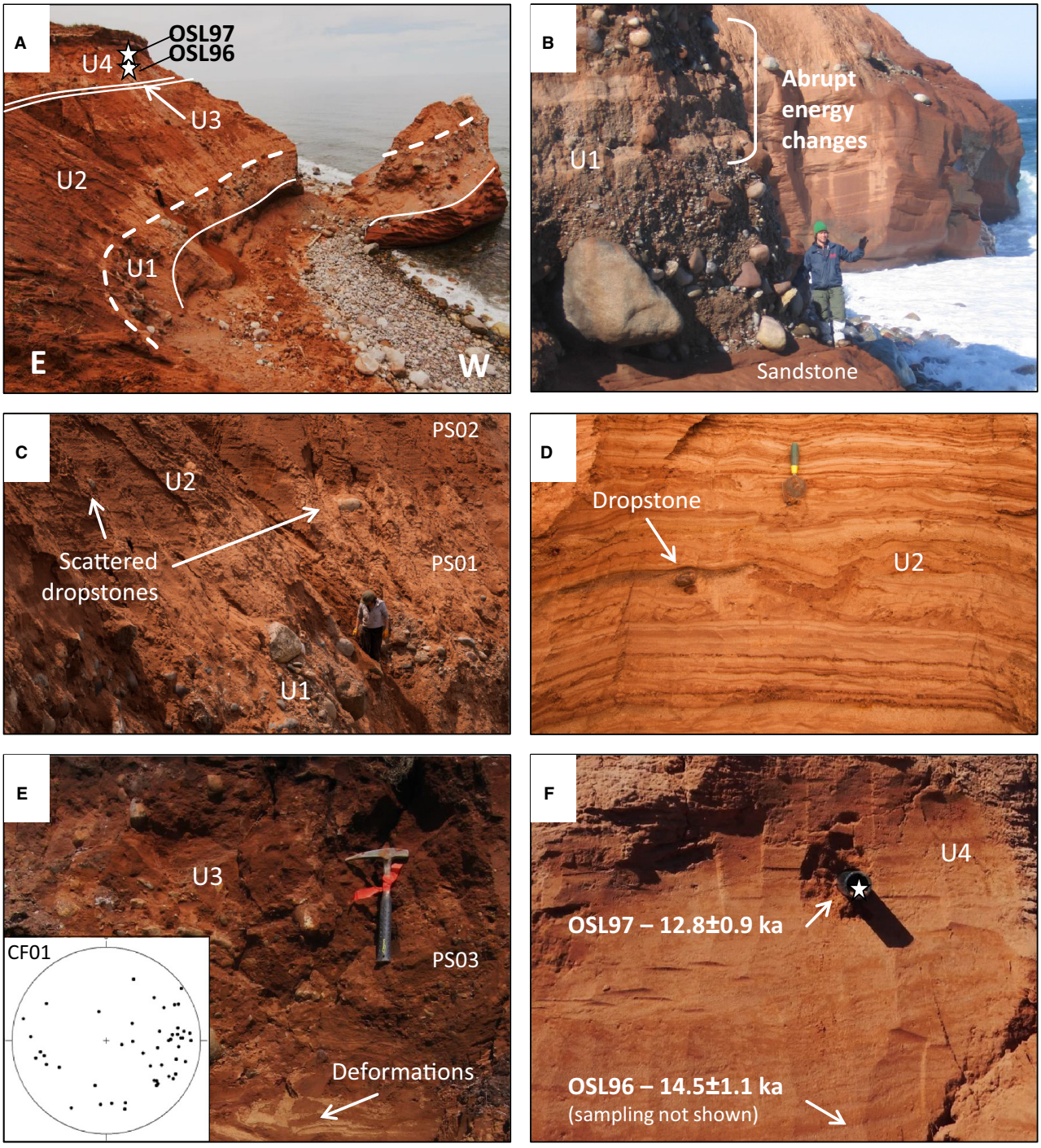

Fig. 4. Representative pictures of the PAL-north site. U1 = proximal fluvioglacial deposit with a lithology from Anticosti Island and Quebec's North Shore; U2 = stratified marine deposit of moderate energy; U3 = till with Appalachian lithology; U4 = stratified subtidal sand. Stars correspond to OSL sample locations. Numbered symbols (e.g. PS01) are particle size samples. A. Overall picture of the PAL-north site. As scale, a person of 155 cm height stands in the outcrop. B. Close-up of U1; imbricated well-rounded pebbles and boulders, alternating with sand and gravel, reflecting abrupt energy changes. C. Gradual transition between U1 and U2 and presence of dropstones within U2. D. Close-up of U2; stratified deposit composed of centimetric sandy beds alternating with millimetric silty beds and presence of dropstones. E. Close-up of U3 where it appears as a till; compact and poorly sorted diamict comprising striated and contoured-shape pebbles. Inset shows the clast fabric measured in U3. F. Close-up of U4; stratified unit composed of well-sorted and well-rounded red and white sand. As scale, the diameter of the black cylinder is 5 cm. Note: OSL96 was collected at the base of U4 (not shown on the picture).

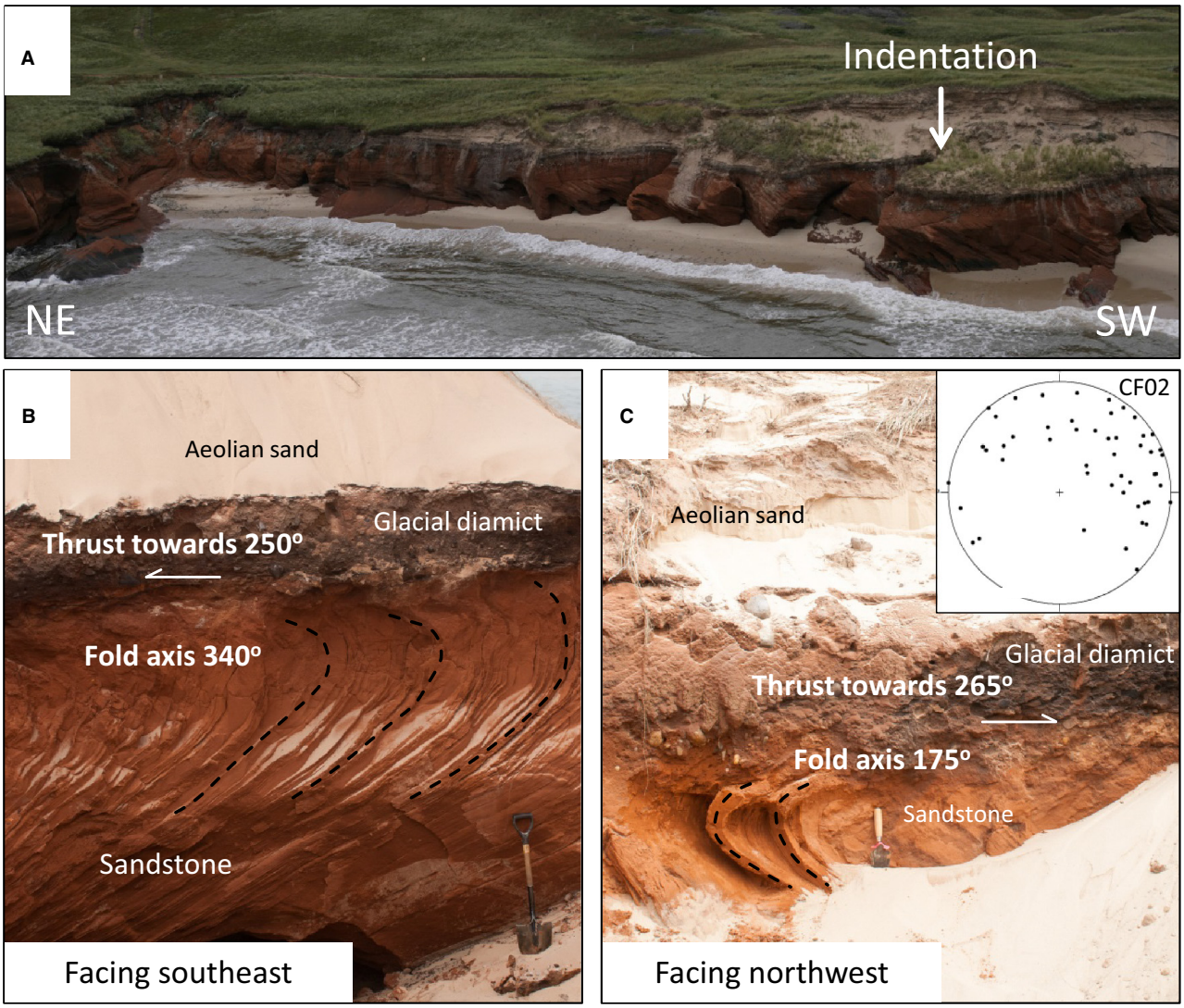

Fig. 5. Representative pictures of the PAL-south site; a till with Appalachian lithology overlies the folded sandstone bedrock. A. Location of the outcrop on the coastal cliff. The total width of the picture is approximately 50 m. B. Outcrop facing the southeast. C. Outcrop facing the northwest. Inset shows the clast fabric measured in the till.

by a ~3-m-thick stratified unit (U4) composed of well-sorted and well-rounded red and white sand (Fig. 4F). U4 is characterized by an alternation of fine white sand and reddish silty-sand (Table S1). The contact between the different beds exposes micro-scale ripple marks. Two samples were collected in U4, OSL96 at the base (+15 m) and OSL97 (+18 m) at the top, giving ages of 14.5±1.1 and 12.8±0.9 ka, respectively (Fig. 4F; Table 2).

The PAL-south exposure is located in an indentation of the sandstone platform (Fig. 5A), allowing the outcrop to be studied on two opposing sides (Fig. 5B, C). The top of the sandstone bedrock is folded and overlaid by a ~80-cm-thick compact and poorly sorted diamict. The fold axes measured on each side of the exposure are consistent with each other (340 and 175°), and reveal a thrust towards the WSW (respectively 250 and 265°) (Fig. 5B, C). A clast fabric measured in the overlying diamict suggests a NE–SW axis (inset Fig. 5C; Table 1). A petrographic count (n = 50) indicates that this unit is mostly allochthonous, with 76% metaquartzite, gabbro and anorthosite, and 22% varied erratic (jasper, granite). The diamict is topped by recent aeolian sediment.

Interpretations. – Owing to the clastic support, the imbrication, the very well-rounded shape of pebbles and boulders (regardless of the nature) and the metric size of several boulders, U1 is interpreted as a proximal fluvioglacial unit (high energy; Dredge *et al.* 1992). U2 is identified as a marine deposit of moderate energy (shallow water); the rhythmicity of beds, probably due to an alternating energy, might reflect seasonality. The conformable contact and the gradual decrease in

particle size between U1 and U2, added to the decrease in concentration of dropstones from the base to the top of U2, strongly suggest a transition from a proximal to a more distal sedimentary source. The dominant lithology of U1 originates from the northern part of the Gulf of St. Lawrence (Anticosti Island and Quebec's North Shore). This fluvioglacial deposit (U1) is thus likely to be associated with a deglacial phase of the Laurentide Ice Sheet (LIS). As the LIS retreated, the glacio-isostatically depressed area was inundated by the sea, and the more distal sedimentary source induced deposition of marine sediments (U2). The absolute age of these events is >130 ka. This sequence is interpreted similarly by Dredge *et al.* (1992); they suggested a pre-MIS 5 age.

U3 corresponds to a typical till (compact, poorly sorted matrix, pebbles with glacial shape, striated pebbles), as suggested by Dredge *et al.* (1992), but with an erratic Appalachian lithology. The E–W axis of the clast fabric added to the Appalachian lithology give a mean orientation towards the west, in contrast to Dredge *et al.* (1992) who suggested a glaciation from the west. The load structures at the top of U2 are also consistent with a glacier loading. The till is overlain by a stratified unit composed of fine sand (U4), interpreted as subtidal deposit associated with a high sea level after the glaciation. The OSL ages suggest that sea level was high at least +18 m between 14.5±1.1 ka (OSL96) and 12.8±0.9 ka (OSL97). The stone line is the result of the till reworking by waves at the high sea-level stage.

The PAL-south exposure is interpreted as the extension of U3 of the PAL-north exposure, namely the Appalachian till. All characteristics are similar: the compactness, the poorly-sorted matrix, the lithology and the clast fabric axis. The WSW orientation of the glaciotectonic deformations in the sandstone and the clast fabric axis are consistent with a glaciation from the east-northeast.

Sandcove–Seacow

This site, located on Grande-Entrée Island (Fig. 1), is a ~300-m-wide active cliff where two different exposures were studied: Sandcove and Seacow (Fig. 6A–C). At the Sandcove site (Fig. 6A), three units were identified. The first unit (U1) is a homogenous sandy deposit with a thickness of at least ~10 m; the underlying contact is unknown. U1 is slightly horizontally stratified: the homogenous fine sand is dominant but alternates with either beds of coarse sand (1–2 cm) or reddish clay (0.5 cm), both slightly inclined (1–3°) towards the SW (Fig. 6D; Table S1). Cross-bedding structures and scattered red clay clasts are also observed within U1. Luminescence measurements using quartz gave a minimum age of >150 ka based on $2\times D_0$ (saturated quartz; OSL26, OSL29; Table 2). U1 is sharply truncated and the contact is marked by a stone line (U2) (Fig. 6A, E). Pebbles in U2 are well rounded and heterometric; some have a diameter >30 cm. A petrographic count was not carried out on the stone line but a visual analysis suggests a foreign origin because of the dominant crystalline lithology (Fig. 6E). Above the stone line, a ~1-m-thick unit (U3) is composed of horizontally stratified, well-sorted and well-rounded fine sand (Fig. 6A, F; Table S1); this unit provides an OSL age of 12.2±0.9 ka (+16 m; OSL72, Fig. 6A, Table 2). The

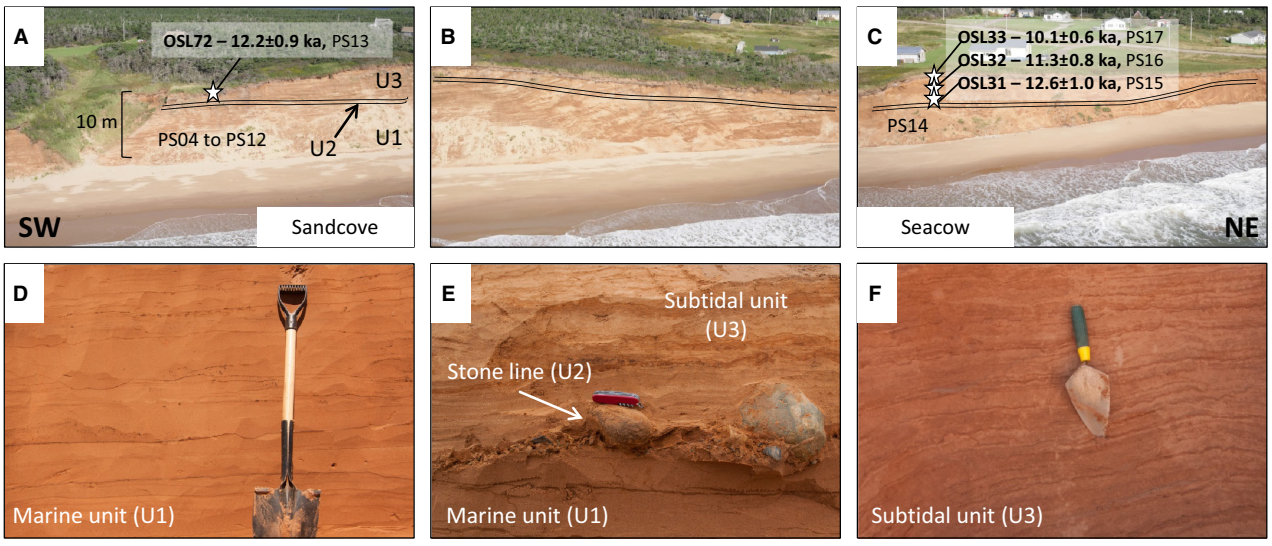

Fig. 6. Representative pictures of the Sandcove–Seacow site. U1 = slightly stratified marine deposit; U2 = stone line of erratic lithology; U3 = stratified subtidal sand. Stars correspond to OSL sample locations. Numbered symbols (e.g. PS14) are particle size samples. A, B and C have a width of ~100 m each. A. The Sandcove site. B. Section between the Sandcove and the Seacow sites. C. The Seacow site. D. Close-up of U1. E. Close-up of U2. F. Close-up of U3.

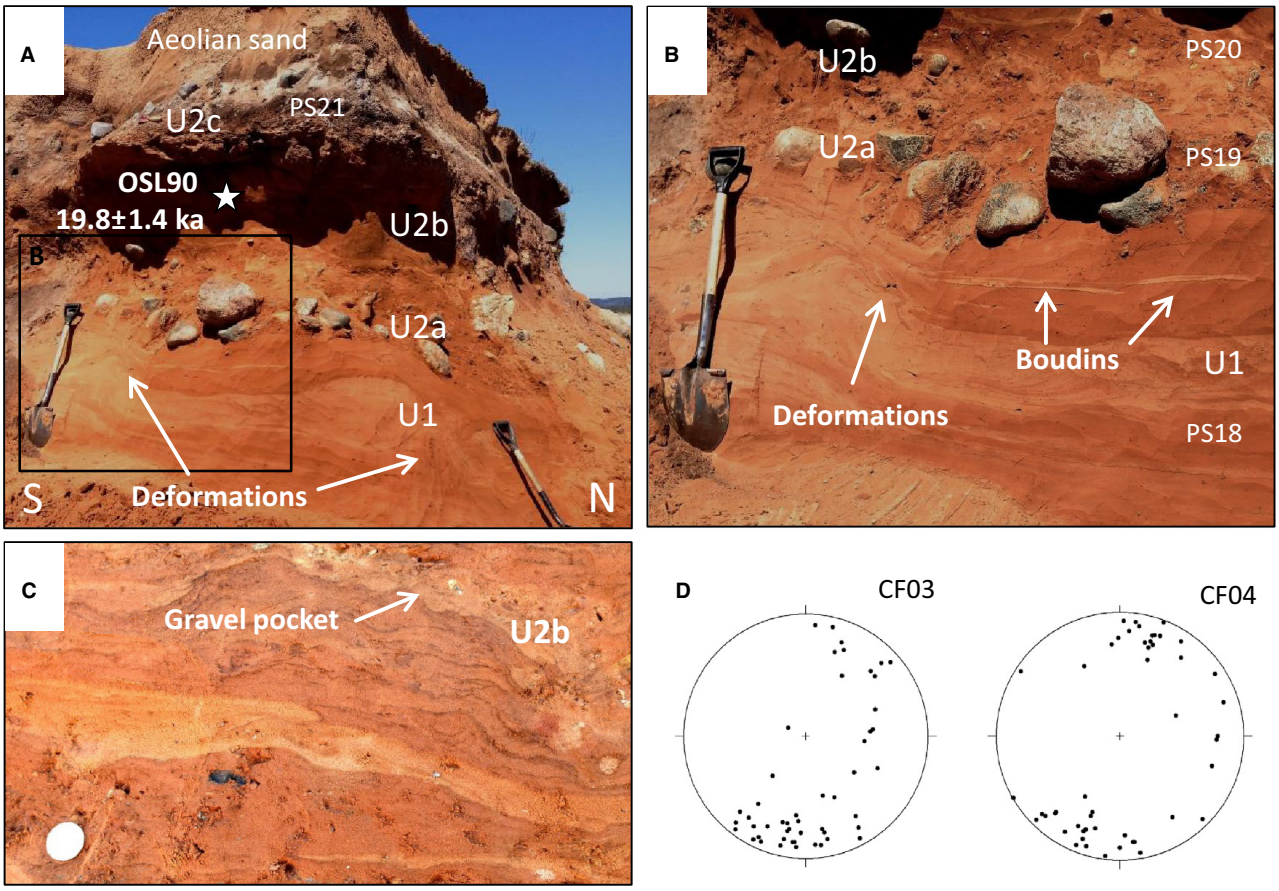

Fig. 7. Representative pictures of the Old-Harry site. U1 = slightly stratified and deformed marine deposit; U2 = till; U2a = till composed of well-rounded erratic pebbles and boulders; U2b = stratified sandy lens within U2 composed of gravel pockets/beds and boudins of whitish sand; U2c = till composed of well-rounded erratic pebbles and boulders. Star corresponds to OSL sample locations. Numbered symbols (e.g. PS18) are particle size samples. A. Overall picture of the Old-Harry site. B. Close-up of U1 illustrating boudins of whitish sand and deformations. C. Close-up of U2b. The coin is ~3 cm diameter. D. Clast fabrics measured in U2.

same three units with very similar characteristics were observed at the Seacow site (Fig. 6C). Quartz luminescence measurements in U1 gave a minimum age of >110 ka (OSL30; Table 2). The thickness of U3 at this site is ~3 m and the deposit displays undulating contacts (micro-scale ripples) between the red beds of silty-sand and the whitish beds composed of fine sand (Fig. 6F; Table S1). Three OSL samples were collected in U3 at the Seacow site and the resulting ages, from the base to the top, are 12.6±1.0 ka (+11 m; OSL31), 11.3±0.8 ka (+12 m; OSL32) and 10.1±0.6 ka (+13 m; OSL33) (Fig. 6C, Table 2).

Interpretations. – Owing to its homogenous facies composed of fine sand (mean = 180 μm; Table S1), U1 is interpreted as a marine unit of >150 ka deposited in relatively shallow water. The depositional environment is characterized by a moderate energy with periods of higher or lower energy, allowing the deposition of respectively coarser sand or clay beds (Fig. 6D). The stone line (U2) separates U1 from U3. The latter is interpreted as a subtidal unit analogous to U4 described at the PAL-north site. The OSL ages also correspond to a post-LGM high sea-level event (at least +16 m between ~13 and 11 ka). The stone line, composed of erratic lithology, might be analogous to U3 at PAL-north and PAL-south, but the lack of quantitative petrographic information does not allow us to interpret it convincingly at this stage.

Old-Harry

The Old-Harry site is located on the eastern part of Grande-Entrée Island (Fig. 1). The exposure comprises two different units lying on the sandstone bedrock (Fig. 7A). The first unit (U1) is ~1 m thick and is composed of moderately sorted, slightly horizontally stratified red and white fine sand (Table S1); the unit is very similar to U1 at the Sandcove–Seacow site. U1 is very compact and displays folded, faulted and boudin structures, as well as sandy pockets (Fig. 7A, B). The measurement of a fold axis suggests

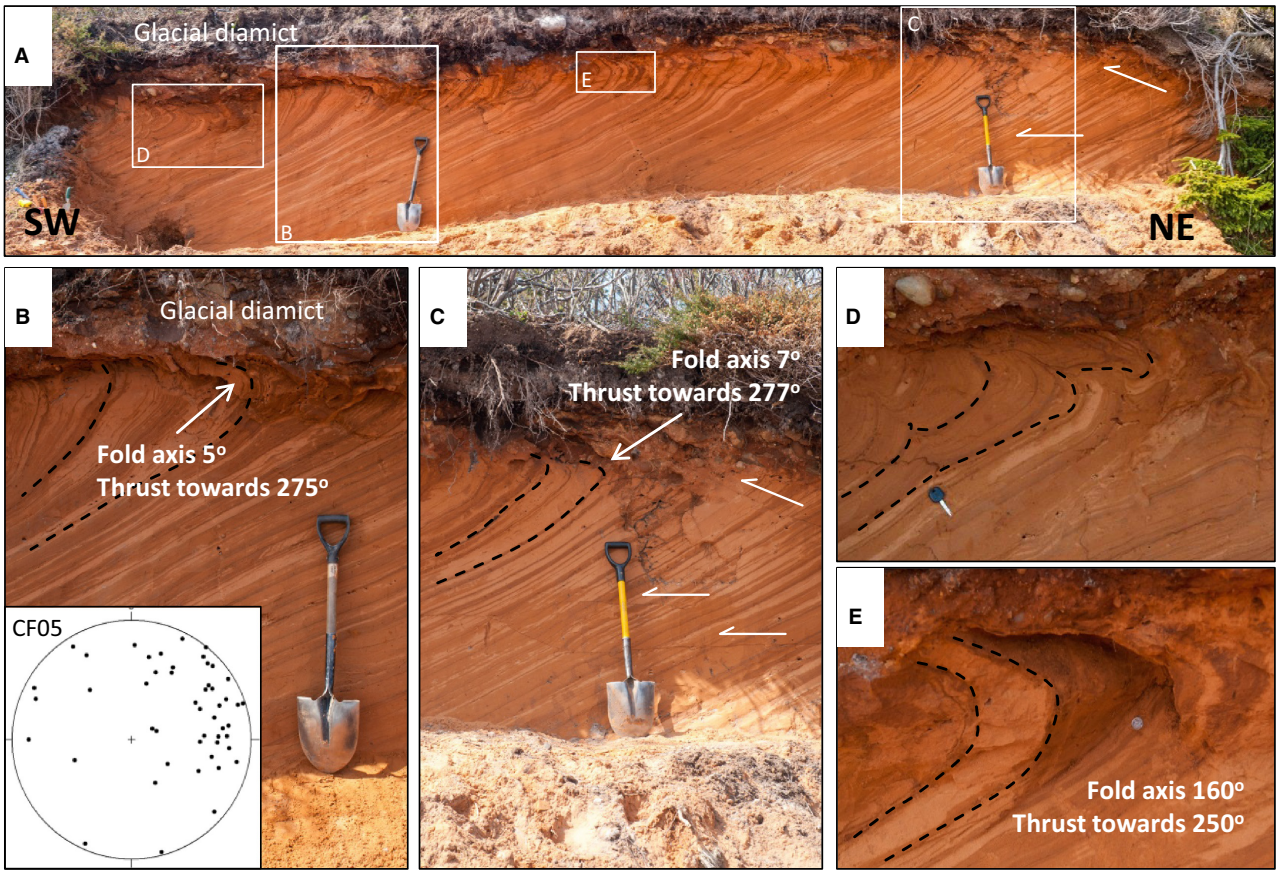

Fig. 8. Representative pictures of the BAH-west site; a till with Appalachian lithology overlies the folded sandstone bedrock. A. Overall picture of the BAH-west site. B. Close-up of a section displaying folded structures of the bedrock under the till. Inset shows clast fabric measured in the diamict. C. Close-up of a section indicating folded and faulted structures. D and E. Close-up of folded structures (as scale, in D, a car key of ~8 cm and in E, a coin of ~2 cm diameter).

a thrust towards 215°. OSL dating provided a saturated age of >170 ka (OSL89; Table 2).

U1 is truncated by the second unit (U2), which appears as a ~2-m-thick diamict separated by a wide lens of sand and gravel (U2b) on a few metres wide (Fig. 7A). The first diamict (U2a) is ~70 cm thick and composed of well-rounded erratic (crystalline) pebbles and boulders. The matrix is very poorly sorted and mostly composed of silty sand (Table S1). The sandy lens (U2b) is ~70 cm thick; the deposit is very compact, stratified and composed of very poorly sorted, very fine sand and coarse silt (Table S1). Gravel pockets/beds were observed in this part of U2 as well as brecciated clay beds and small boudins of whitish sand (Fig. 7C). Many sandy lenses are undulating over and under pebbles. An OSL sample was taken in a sandy part of U2b and the resulting age is 19.8±1.4 ka (OSL90; Table 2). The same diamict (U2c) as U2a covers the U2b lens (~50 cm thick) (Fig. 7A; Table S1). Two clast fabrics (n = 100) were measured in U2a and a mean vector of 198° was determined (Fig. 7D; Table 1). The sequence is topped by an accumulation of recent aeolian sediment.

Interpretations. – The first unit (U1) of the Old-Harry exposure is interpreted as marine sediment (relatively shallow water) older than 170 ka. The syngenetic stratifications of U1 are deformed near the contact with U2. U2a and U2b correspond to a single unit interpreted as a till owing to its compactness, the very poorly sorted matrix and the erratic rounded pebbles and boulders. The clast fabrics measured in the till suggest an ice flow towards the SSW, consistent with the deformations in the upper part of U1. U2b is presented as a lens of a few metres wide within the till. The stratifications and the sandy lenses undulating over and under pebbles involve the presence of water at deposition; the presence of water at the base of the glacier indicates a warm-based glacier. The OSL age of 19.8±1.4 ka (OSL90) acquired from the sandy lens indicates that the till was deposited at or later than the end of the LGM.

Bassin-aux-Huîtres (BAH)-West

The Bassin-aux-Huîtres (BAH)-west site is located in the central part of Grande-Entrée Island (Fig. 1). The

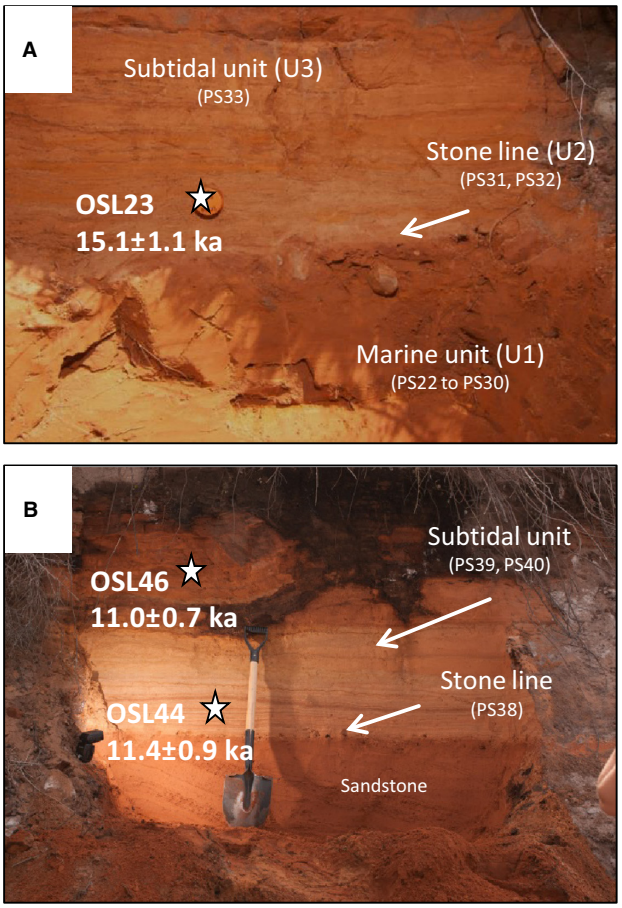

Fig. 9. Representative pictures of the supplementary outcrops on the northern archipelago. Stars correspond to OSL sample locations. Numbered symbols (e.g. PS38) are particle size samples. A. The Bluff-east site. U1 = slightly stratified marine sand; U2 = till or stone line composed of erratic well-rounded pebbles and boulders; U3 = stratified subtidal sand. As scale, the orange cap is ~5 cm diameter. B. The Airport site; stratified subtidal sand overlying the sandstone bedrock. The contact is marked by a stone line of far-travelled origin.

BAH-west site exposes many deformations of the sandstone bedrock topped by a compact diamict (Fig. 8A). The deformed bedrock is exposed on a ~10 m wide and ~1.5 m high from the modern high tide level, where at least three reverse faults are visible (Fig. 8A, C). The translational movement of the upper part is approximately towards the WSW (Vigneault 2012). The top part of the sandstone is entirely folded. Fold axes of 5, 7 and 160° were measured at three different places, involving a westward thrust (respectively 275, 277 and 250°) (Fig. 8B, C, E). The overlying diamict is composed of varying sized rounded to well-rounded pebbles and boulders. A petrographic count carried out on a few pebbles (n = 25) suggests a foreign origin: 64% metaquartzite, gabbro and anorthosite, 16% jasper and 20% varied erratics such as gneiss, granite and schist. Clast fabric measurements (n = 50) revealed an ENE–WSW depositional direction (inset Fig. 8B; Table 1).

Interpretations. – The BAH-west site exposure is interpreted as a till covering the bedrock. The WSW orientation of folds and reverse faults are consistent with the clast fabric, suggesting that deformations of the sandstone have a glaciotectonic origin. The WSW orientation and the Appalachian lithology are similar to the PAL-north and PAL-south sites.

Supplementary outcrops on the northern archipelago

Three more exposures complete the overall picture for the northern archipelago: Bluff-east, Bassin-aux-Huîtres (BAH)-east and Airport (Fig. 1). The Bluff-east site exposes three different units (Fig. 9A). The first unit (U1) is composed of slightly stratified, fine to very fine sand (Table S1). A minimum age of >110 ka was derived from the saturated quartz (OSL20 and OSL22; Table 2). Deformed millimetric beds of clay are observed as well as centimetric beds of coarser sand and red clay clasts. U1 is at least ~8 m thick (the underlying contact is unknown) and is truncated by a massive diamict that appears as remnant pockets or a stone line (U2). The matrix of U2 is very poorly sorted and the pebbles and boulders have a well-rounded contoured shape and an erratic crystalline origin. Clast fabric and petrographic counting are not available for U2 at this site. U2 is overlaid by a stratified unit of silty sand (Table S1) showing ripple marks dated to 15.5±1.1 ka (+16 m; OSL23) (Table 2).

The BAH-east exposure also displays three units. The first unit (U1) is similar to U1 at the Bluff-east site but is highly deformed (reverse faults and overturned folds), indicating a thrust towards the WSW (Vigneault 2012). U1 is truncated by a compact, poorly sorted diamict (U2) also similar to U2 at the Bluff-east site. Clast fabrics measured in U2 suggest an ENE–WSW/E–W axis (Table 1) consistent with the underlying U1 deformations. A petrographic count (n = 50) reveals that 64% of the pebbles correspond to metaquartzite, gabbro and anorthosite whereas the rest is composed of varied erratics (schist, gneiss, etc.; Vigneault 2012). A ~50-cm-thick stratified silty unit (U3) overlies U2. An age of 10.9±0.8 ka (+4 m; OSL79; Table 2) was measured in U3.

The Airport site is the most 'southerly' site of the northern archipelago (Fig. 1). A stratified unit of well-rounded white and red sand rests directly on the sandstone bedrock (Fig. 9B; Table S1). Two OSL ages were obtained in this unit: 11.4±0.9 ka at the base (+2 m; OSL44) and 11.0±0.7 ka at the top (+3 m; OSL46) (Table 2). The contact between the sandstone and the sandy unit is marked by a stone line of foreign crystalline origin (visual analysis) with a poorly sorted

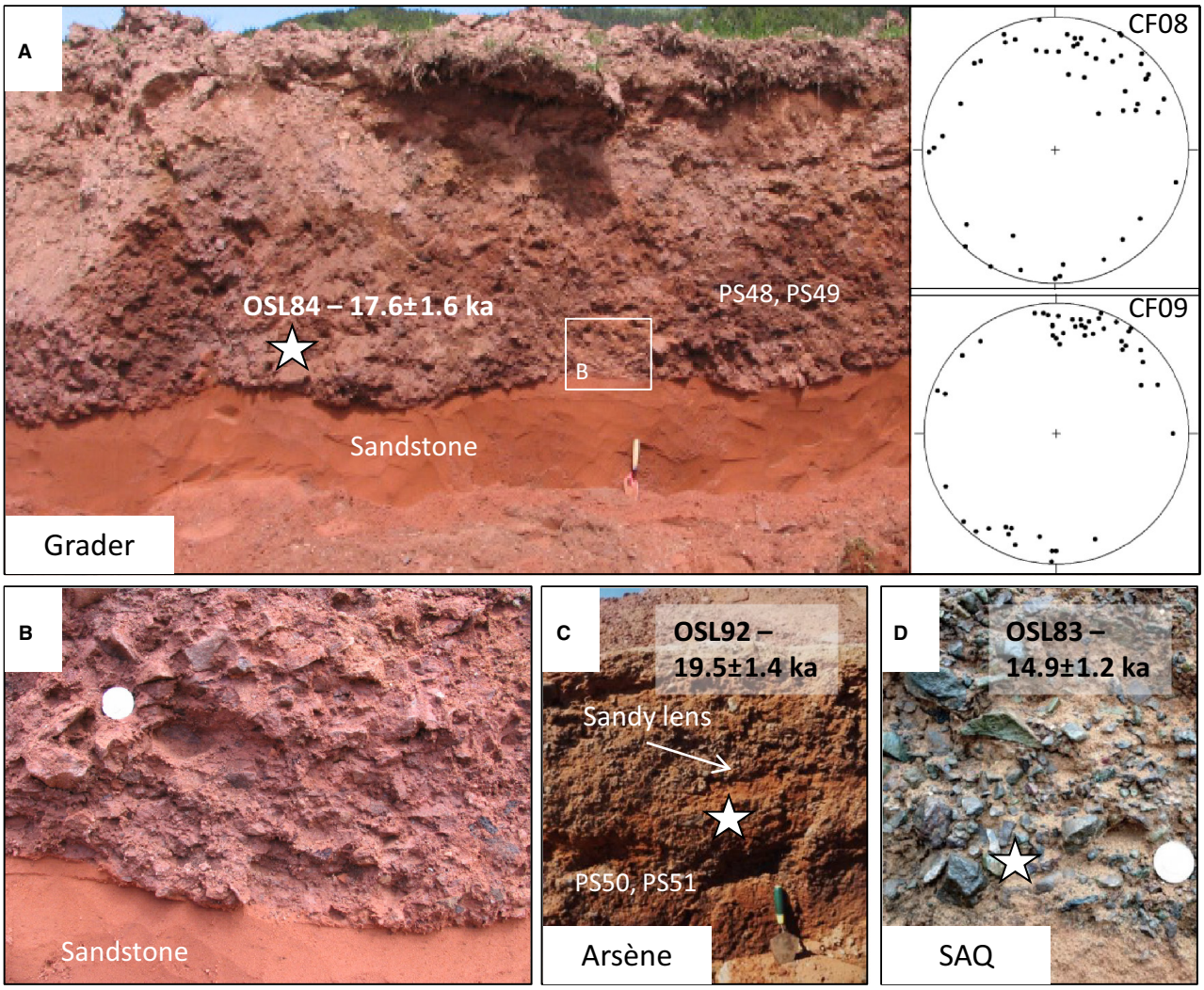

Fig. 10. Representative pictures of the Grader, Arsène and SAQ sites; these sites present clast-supported and moderately sorted compact diamict comprising exclusively angular pebbles of unstriated local basalts interpreted as cryopediments. Stars correspond to OSL sample locations. Numbered symbols (e.g. PS48) are particle size samples. The coin in B and D is ~3 cm diameter. A. The Grader site. Inset illustrates clast fabrics measured in the diamict. B. Close-up of the undulating contact between the sandstone bedrock and the diamict at the Grader site. C. The Arsène site. D. The SAQ site.

matrix (Table S1). Pebbles in this unit are smaller compared with the other sites on the northern archipelago; no boulders are visible.

Interpretations. – U1 at both the Bluff-east and BAH-east sites are interpreted as marine sediment deposited in shallow water. The minimum age acquired in U1 at the Bluff-east site suggests a deposition before *c.* 110 ka. At the Bluff-east site, the slight deformations in U1 are likely to have a subaqueous origin whereas the reversed faults and overturned folds in U1 at the BAH-east site are more likely to have a glaciotectonic origin; the deformation orientations in U1 are consistent with the clast fabrics of the overlying diamict (U2). At the three sites, the diamict (stone line at the Airport site) is interpreted as a till and the Appalachian lithology suggests a glacial movement towards the W or WSW. U3 at both Bluff-east and BAH-east, as well as the main unit at the Airport site, is interpreted as a subtidal unit deposited during a post-LGM high sea level of at least +16 m. The OSL ages from the three sites indicate that this high sea level occurred at least between 15.5±1.1 ka (OSL23) and 10.9±0.8 ka (OSL79) (Table 2).

Havre-Aubert and Cap-aux-Meules Islands

Grader, Arsène and SAQ sites. – These three inland sites represent temporary surface excavations located in a gentle slope (<3°): Grader (+50 m), Arsène (+50 m) and SAQ (+10 m) (Fig. 1). At the three sites, the unit lies directly on the sandstone bedrock and

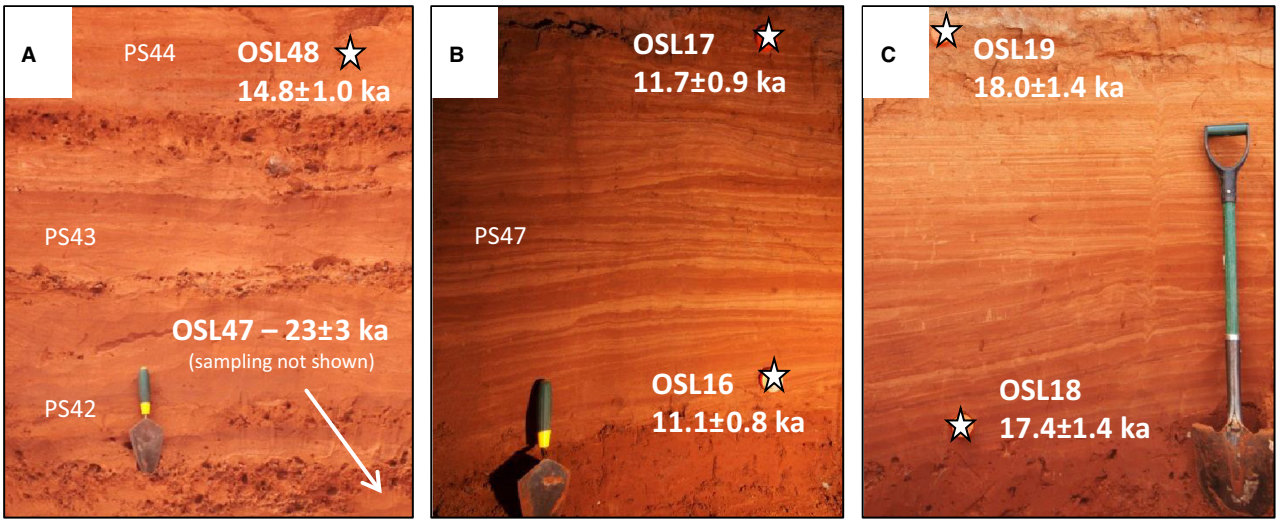

Fig. 11. Representative pictures of the southern archipelago; these sites present stratified very fine to silty red and white sand. Stars correspond to OSL sample locations. Numbered symbols (e.g. PS42) are particle size samples. A. The Fatima site; this site exposes stratified fine sand with gravel beds. B. The AP-DEM site. C. The AP-CAM site.

corresponds to a ~1–1.5 m thick clast-supported and moderately sorted compact diamict comprising exclusively angular pebbles of unstriated local basalts (Fig. 10). The contact between the sandstone and the unit is characterized by an undulating shape (channelized; Fig. 10A). The unit also includes variably sized lenses of brownish sand (Fig. 10C). Two clast fabrics were measured (n = 99) at the Grader sites and the data illustrate a concentration of orientations around the mean vectors (azimuth of ~15° and 22°), which is parallel to the slope (~195±5°) (inset Fig. 10A; Table 1). Each site was sampled for OSL dating and the resulting ages are 17.6±1.6 ka (Grader, OSL84; Fig. 10A), 19.5±1.4 ka (Arsène, OSL92; Fig. 10C), and 14.9±1.2 ka (SAQ, OSL83; Fig. 10D) (Table 2).

This clast-supported diamict composed exclusively of unstriated local basalts is interpreted as a periglacial colluvial deposit (cryopediments; Paquet 1989); the angular clasts are produced by frost-shattering of the central hills. At the Grader site, the central hills are located roughly to the north of the exposure, which is consistent with the N–S orientation of the clast fabrics (parallel with the slope). Cryopediments need the presence of perennially frozen ground to block the infiltration of water leading to surface flow forming slightly inclined (<3°) morphologies (e.g. Vandenberghe & Czudek 2008). The channel-shaped sandy lenses observed within the diamict testify that runoff played a role in the deposition. The post-LGM ages acquired at the three sites argue for periglacial conditions after the LGM glaciation.

Southern archipelago stratified sand. – A sandy deposit is ubiquitous on the southern archipelago at variable elevations: Havre-aux-Maisons (HAM; +9 m), Fatima (+6 m), AC-Lighthouse (+13 m), ACW (+24 m), AP-CAM (+13 m) and AP-DEM (+15 m) (Fig. 1). The thickness of the unit varies from site to site between 0.3 and 3 m and is composed of horizontally stratified, moderately sorted very fine to silty red and white sand (Fig. 11; Table S1). Cross-bedding structures and micro-scale ripple marks are also observed in the unit. At a few sites, the sand is somewhat coarser and gravel beds are observed within the unit (e.g. Fig. 11A). At the HAM, Fatima (Fig. 11A) and AC-Lighthouse sites (Fig. 2A), the unit lies on the bedrock (sandstone or argillite), whereas at ACW, AP-DEM (Fig. 11B) and AP-CAM (Fig. 11C), the unit overlies the Drift des Demoiselles, an MIS 2 glaciomarine deposit described by Rémillard *et al.* (2013). Many OSL ages were acquired at different altitudes from these sites in the stratified sand: 23.0±1.6 ka at HAM (OSL63), 23±3 ka (base) and 14.8±1.0 ka (top) at Fatima (OSL47 and OSL48; Fig. 11A), 38±3 ka (base) and 9.8±0.6 ka (top) at AC-Lighthouse (OSL08 and OSL12), 11.6±0.7 ka at ACW (OSL06), 11.1±0.9 ka (base) and 11.7±0.9 ka (top) at AP-DEM (OSL16 and OSL17; Fig. 11B), and 17.4±1.4 ka (base) and 18.0±1.4 ka (top) at AP-CAM (OSL18 and OSL19; Fig. 11C) (Table 2). A radiocarbon age of 10.20±0.03 cal. ka BP (UCIAMS-134737; Table 3) was also acquired at the AC-Lighthouse site (Fig. 2A). As mentioned in the *Reliability of the OSL ages* section, the only irregularity is the ages of 38±3 ka (base) and 9.8±0.6 ka (top) at the AC-Lighthouse site (OSL08 and OSL12) for which we believe a misidentification in the field led to this stratigraphical inconsistency.

This stratified unit of very fine sand is interpreted as a subtidal deposit. The small variations in particle size (silty sand to sand with gravel beds) reflect the variable

coastal energy around the islands. Both sedimentological facies and ages are similar to U4 of the PAL-north site, U3 of the Sandcove–Seacow site, etc. The ages are all from MIS 2 and are discussed in the *Post-LGM sea-level variations* section.

Galet-Plat and Gros-Cap sites. – These two sites are located on the southeast side of Cap-aux-Meules Island (Fig. 1). The Galet-Plat exposure comprises a ~30-cm-thick, uncompacted, matrix-supported sandy-gravel deposit that rests directly on the highly weathered sandstone bedrock. The deposit is structureless and composed of local (basalt) subangular to subrounded gravel and pebbles in a poorly sorted sandy matrix, with few well-rounded erratics. This unit is visible over a distance of several kilometres along the coast in this area and two samples were collected for OSL dating at two different places; OSL80 (+6 m) and OSL81 (+4 m) yielded ages of 17.9±1.4 and 21.1±1.7 ka, respectively (Table 2). At the Galet-Plat site, the interface between the bedrock and the gravel unit displays tapered upward-extending injections, round bulges and, downward-extending lobes (involutions). At the Gros-Cap site, a ~20-cm-thick and ~7-m-wide compact diamict lies between the bedrock and the sandy-gravel deposit described above (Fig. 12). The top of the sandstone bedrock at this location displays many faults and folds whose axes were measured around 310°, suggesting a southwestward thrust (Fig. 12). A clast fabric (n = 30) measured in this diamict also revealed a thrust from ~40° (NE; Table 1).

The uncompacted nature of the gravelly deposit described at the Galet-Plat site and its composition of subrounded, mostly local pebbles in a sandy matrix suggest a coastal environment. The unit is interpreted as a former pebbly beach/subtidal deposit reworked by periglacial processes (cryoturbations; Rémillard *et al.* 2015a). At the Gros-Cap site, the thin diamict squeezed between the deformed sandstone bedrock and the coastal deposit is interpreted as a remnant lens of a till. The faults and the folds at the top of the sandstone bedrock are interpreted as glaciotectonic deformations; their orientations are consistent with the clast fabric measured in the till. The latter was most likely of a greater extent but the high sea level, attested to by the overlying coastal deposit, washed the till recurrently, leaving only a thin lens behind. The OSL ages of 17.9±1.4 and 21.1±1.7 ka obtained in the coastal deposit suggest an early deglaciation of this part of the Magdalen archipelago and a post-LGM higher sea level. The remnant till is therefore older and could have been deposited during the LGM or earlier.

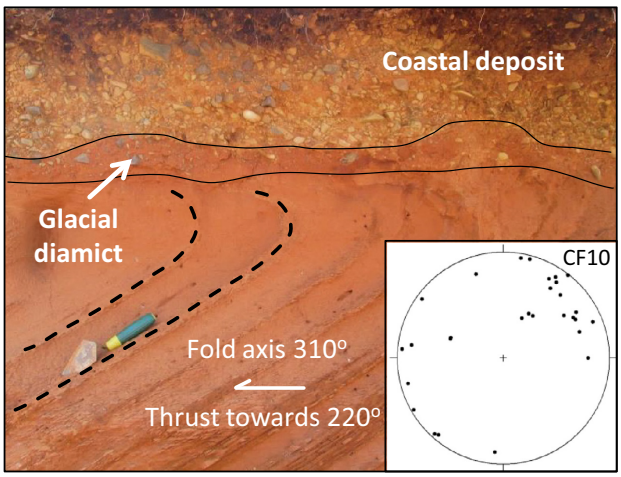

Fig. 12. Representative picture of the Gros-Cap site. The sandstone bedrock is folded and overlaid by a thin and compact till and a coastal deposit composed of mostly local (basalt) subangular to subrounded gravel and pebbles in a poorly sorted sandy matrix. Inset illustrates the clast fabric measured in the till.

Clermont site. – The Clermont site is located on the east side of Le Bassin on Havre-Aubert Island (Fig. 1). This site displays a ~2-m-thick organic sequence from the modern high tide level. The deposit sits on an unidentified clayish unit and is composed of varied organic detritus such as plant fragments, and tree branches and trunks; some of which have a diameter of more than 10 cm and were identified as birch trunks. A basal sample gave an age of 10.7±0.1 cal. ka BP (UCIAMS-134729; Table 3).

The organic deposit at the Clermont site is interpreted as an early Holocene terrestrial peat deposited while the sea level was below the current level. Dredge *et al.* (1992) also mentioned a terrestrial peat on the eastern side of Le Bassin, but the site is not localized in their paper. They also acquired a basal age of 10.8±0.4 ka cal BP at −2.2 m.

Discussion

Glacial movements during the LGM

A till was observed at six different exposures in the northern part of the Magdalen Islands: PAL-north, PAL-south, Old-Harry, BAH-west, BAH-east and Bluff-east (Fig. 1). From site to site, the till characteristics are very similar, suggesting that these deposits are probably all from the same glacial event. The till stratigraphical position is recurrent; it always rests either on the bedrock or on a marine deposit older than *c.* 170 ka (based on $2\times D_0$ for sample OSL89). The latter scenario occurs where exposures are located in a bedrock depression, allowing the preservation of older sediment (e.g. Fig. 4). In addition, glaciotectonic deformations were observed in either the bedrock or the marine sediment that underlie the till. The measurements carried out on these deformations show a thrust orientation towards the WSW (~255° on average; e.g. Figs 5, 8). Clast fabrics measured in the till at

different sites revealed that the mean vectors are mostly orientated ENE–WSW; the data provide a concentration of orientations around a mean vector of azimuth ~68° and plunge ~17° (Table 1). Clast fabrics have been the subject of much discussion and have to be considered cautiously; some authors argue that they are not good indicators of ice flow (e.g. Carr & Rose 2003; Evans *et al.* 2006). However, we note that most mean vectors are orientated along the ENE–WSW axis, which is consistent with the ice-flow direction towards the WSW suggested by the glaciotectonic deformation structures. Taken together, these data strongly suggest an ice flow from the ENE, which is in opposition to Dredge *et al.* (1992) who suggested a glaciation from the west.

The allochthonous petrography is also very similar from site to site. The petrographic counts undertaken at the PAL-north, PAL-south, BAH-west and BAH-east sites indicate that ~70% of the pebbles are metaquartzite, gabbro and anorthosite. The remaining are granitoids (granite, gneiss) and variable erratics such as jasper, chert, phyllite and schist. These assemblages are typical of Appalachian lithology (Vigneault 2012). At the PAL-north and Bluff-east sites, the till appears rather as remnant pockets that evolve laterally as a stone line. The overlying subtidal unit suggests that the till has been reworked by coastal processes during a higher sea level. At the Seacow–Sandcove and Airport sites, the stone line is overlain by a subtidal deposit and although no petrographic counting is available, visual analyses suggest that the lithology is similar to the till described above. We therefore interpret the stone line at these three sites as the remnant part of the Appalachian till. The clast fabric and glaciotectonic deformation orientations added to the Appalachian lithology point to a glaciation from the Newfoundland icecap. From here, we suggest the name of Grande-Entrée till to refer to the till of the northern Magdalen Islands.

The stratigraphical data reveal that the extension of the Grande-Entrée till is almost continuous from Havre-aux-Maisons Island (Airport site) to Grande-Entrée Island (Fig. 1). However, the Gros-Cap site displays glaciotectonic deformations and a small lens of till that are both self-consistent and also consistent with ice flow from Newfoundland. Although the evidence is limited, it suggests that the glacial movement might have reached at least the eastern part of Cap-aux-Meules Island.

The timing of the Newfoundland ice flow on the northern Magdalen Islands is constrained by an OSL age of a sand lens in a glacial till at the Old-Harry site: 19.8±1.4 ka (OSL90; Table 2). At two standard deviations, the age bracket is 22.6–17 ka, which covers the LGM period. OSL dating of glacial deposits is a subject of discussion because of the possibly poor bleaching at deposition (e.g. Fuchs & Owen 2008). Here, had the sediment not been well bleached at deposition, the age of 19.8±1.4 ka would be an overestimate, meaning that the glaciation would probably be younger. This scenario is improbable because according to the regional literature, the Laurentian Channel in the Gulf of St. Lawrence was entirely deglaciated around 17 cal. ka BP (e.g. Shaw *et al.* 2006; Stea *et al.* 2011), making a later ice flow from Newfoundland unlikely. In addition, the Grande-Entrée till or stone line is overlain at many sites by a subtidal deposit dated between 15.1±1.1 ka (OSL23) and 10.1±0.6 ka (OSL33) (Table 2), again suggesting that the northern part of the Magdalen Islands was indeed deglaciated after *c.* 17 ka.

On Havre-Aubert Island, which is the most southerly island of the archipelago (Fig. 1), Rémillard *et al.* (2013) described a southeastward ice movement during the MIS 2. This ice flow is interpreted as originating from the Escuminac icecap, whose centre of dispersion was located in the northwestern part of the Gulf of St. Lawrence. The precise age of this ice flow is unknown, but as the glacial diamict lies on a MIS 3 deposit dated by both radiocarbon (Rémillard *et al.* 2013) and OSL (Fig. 2B), it is very likely that the glacial movement occurred during MIS 2 and most probably during the LGM. Rémillard *et al.* (2013) observed this glacial deposit at two different sites only on Havre-Aubert Island, but other authors described a very similar diamict on the southwestern part of Cap-aux-Meules Island (Paquet 1989; Dredge *et al.* 1992) (Fig. 1). In our study, the results strongly suggest that the glacial evidence on the northern archipelago is totally distinct from the southern indications. The glaciotectonic deformation and clast fabric orientations are to the west–southwest for the northern islands whereas they are southeastward for the southern part of the archipelago (Rémillard *et al.* 2013). Furthermore, the petrography of the till is far-travelled in the northern archipelago (Vigneault 2012) and local (sandstone and basalt) on Havre-Aubert Island (Rémillard *et al.* 2013). There seems no doubt that these two glacial diamicts were deposited by two different ice flows that reached the Magdalen Islands during the MIS 2; this result is in contrast to that of Dredge *et al.* (1992) who suggested a MIS 4 age for the last glacial movement that reached the archipelago and a long cold period for MIS 2.

According to our observations at the Gros-Cap site, and taking into account the descriptions of Paquet (1989) and Dredge *et al.* (1992), it seems that both ice movements from the Escuminac and Newfoundland icecaps touched Cap-aux-Meules Island. However, it is not possible at this stage to make any assumptions about whether the icecaps were synchronous. Another peculiar observation on Cap-aux-Meules Island is the very well-developed periglacial landforms, i.e. cryopediment surfaces and dry and asymmetrical valleys (e.g.

Paquet 1989). Based on a detailed analysis of ice-wedge pseudomorphs, composite-wedge casts and cryoturbation structures, Rémillard *et al.* (2015a) suggested that permafrost developed after the LGM glaciation, and that the archipelago then remained under periglacial conditions for a prolonged period. Here, our results revealed that the ages of the three cryopediment deposits observed on Cap-aux-Meules Island are between 19.5±1.4 ka (OSL92) and 14.9±1.6 ka (OSL83) (Table 2). These ages are consistent with the interpretation of Rémillard *et al.* (2015a) and suggest that as soon as Cap-aux-Meules Island was deglaciated after the LGM, periglacial processes occurred, allowing the development of cryopediment surfaces, ice wedges, etc. As the ice margins of both the Escuminac and Newfoundland icecaps were on Cap-aux-Meules Island during the MIS 2, it might have been the first ice-free island and therefore the first to be affected by periglacial conditions, explaining the well-developed periglacial landscape and the ages between *c.* 15 and 20 ka for the cryopediments. The periglacial landscape is also well developed on Havre-Aubert and Havre-aux-Maisons Islands (Laverdière & Guimont 1974; Paquet 1989; Rémillard *et al.* 2015a), suggesting that these islands were probably also deglaciated immediately after the LGM. Finally, the age of 19.8±1.4 ka (OSL90) obtained on the Grande-Entrée till at the Old-Harry site suggests that the northern archipelago was still ice-covered while the southern part was deglaciated and affected by periglacial processes.

Post-LGM sea-level variations

Throughout the Magdalen Islands there is a ubiquitous stratified fine sand deposit interpreted as a subtidal deposit. On the northern archipelago, this unit is always observed above the Grande-Entrée till or the stoneline (e.g. U4 at the PAL-north site). The ages from this subtidal unit range between *c.* 15 and 10 ka, stratigraphically consistent with the age of 19.8±1.4 ka associated with the underlying Grande-Entrée till. In the southern part of the archipelago, the ages obtained from the subtidal unit also fall into the post-LGM period (Table 2). However, a few exposures provide ages of between *c.* 18 and 23 ka, i.e. the AP-CAM, Galet-Plat, HAM and Fatima sites. Even at two standard deviations, these ages are older than those obtained on the northern part of the Magdalen Islands, as well as the dated cryopediment surfaces discussed in the previous section; they suggest an earlier deglaciation of the south islands (Havre-Aubert, HAM and Cap-aux-Meules Islands).

Subtidal deposits are less accurate indicators of relative sea-level (RSL) elevation than littoral deposits; subtidal deposits merely testify that the sea level was higher than their current altitude. On the Magdalen Islands, altitudes associated with this subtidal unit vary from 2 to 24 m; for just these two elevations the ages are quite similar: 11.4±0.9 ka (OSL44) and 11.6±0.7 ka (OSL06), respectively. The age variability for this single unit is explained by the different locations and elevations of the sites, and by the different glacial history of the islands, which influences the subsequent sea-level variations differently. Figure 13 illustrates a preliminary post-LGM RSL variation curve based on the different OSL ages acquired on the subtidal unit throughout the archipelago. The basal age of 10.7±0.1 cal. ka BP (UCIAMS-134729) in the terrestrial peat at the Clermont site together with the age of 10.8±0.4 cal. ka BP (GSC-4565) obtained at −2.2 m in the same area by Dredge *et al.* (1992) suggest that the sea level passed below the current level just prior to 10.7 cal. ka BP (Fig. 13; Table 3). A ~60-cm-thick organic horizon containing leaves and tree trunks was found by the Canadian Salt Company Seleine Mines at a depth of 17 m under current sea level when they drilled for a well (Anonymous 1981). A radiocarbon age of *c.* 9.8 cal. ka BP was obtained from a well-preserved piece of wood recovered from this horizon (represented by the cross in Fig. 13). The sea level was necessarily lower than −17 m at that time but it is impossible to speculate on the exact depth.

Considering the four postglacial RSL scenarios proposed for Atlantic Canada (Quinlan & Beaumont 1981; Dyke & Peltier 2000; Shaw *et al.* 2002), our data indicate that the Magdalen Islands are consistent with scenario B (J-shaped curve) although we do not provide precision for the period between *c.* 25 and 12 ka (Fig. 13). This scenario proposes that the RSL was initially higher than the current sea level, after the deglaciation, because of the glacio-isostatic depression. Then, the RSL dropped below the current sea level due to the isostatic rebound and reached a postglacial sea-level lowstand during the passage of the marginal forebulge crest. The sea level rose again to reach the current level because of the subsidence associated with the glacial isostatic adjustment. The initial elevation, the timing of the passage below current level, the depth of the low level as well as the timing of the rise are all data that vary spatially and temporally at the scale of Atlantic Canada. For instance, Kelley *et al.* (2011) stated that between *c.* 16 and 12 cal. ka BP, the RSL fell from +70 to −60 m in the Gulf of Maine, which is earlier than what we observe in the Magdalen Islands. This significant decrease in RSL is associated with a very rapid passage of the peripheral forebulge after the deglaciation of this area (Barnhardt *et al.* 1995). On the inner Scotian Shelf, the postglacial sea-level lowstand reached −65 m around 13 ka (11.6 uncal. ka BP) (Stea *et al.* 1994, 1998). On the western coast of Newfoundland, in the St George's Bay area, the RSL reached +27 to +105 m around 16.4 cal. ka BP

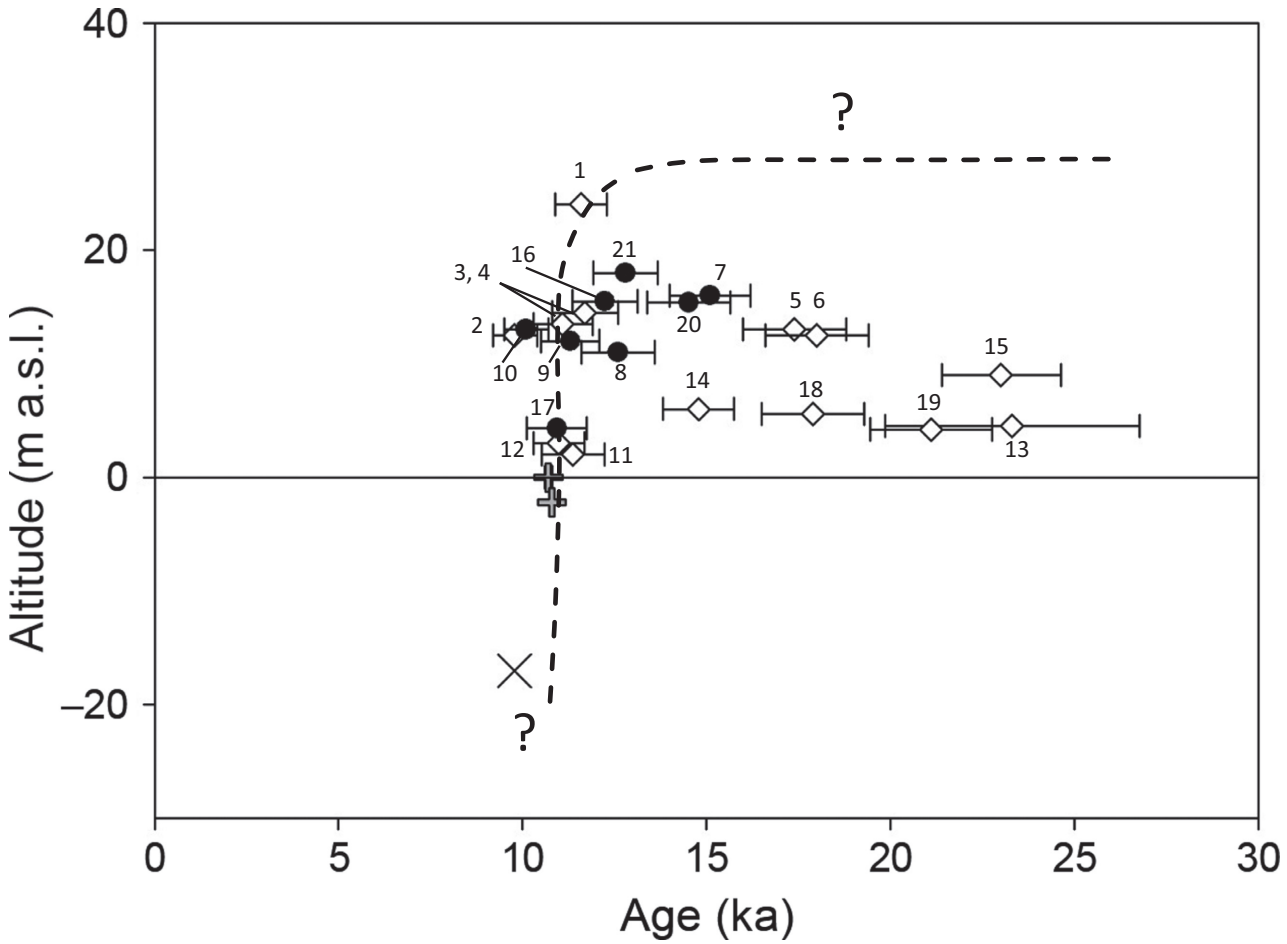

Fig. 13. Preliminary post-LGM RSL variation curve based on the different OSL ages acquired on the subtidal unit throughout the Magdalen Islands (age ±1σ). Unfilled diamonds represent the ages from the southern archipelago (Havre-Aubert, Cap-aux-Meules and Havre-aux-Maisons Islands). Filled circles correspond to the ages from the northern archipelago (Pointe-aux-Loups and Grande-Entrée Islands). Index numbers correspond with Table 2 in order to refer to the specific site, age and elevation of each point. The grey plus symbols represent the terrestrial peat dated to 10.7 cal. ka BP at modern level and to 10.8 cal. ka BP at −2.2 m by Dredge *et al.* (1992). The cross indicates a radiocarbon age of *c.* 9.8 cal. ka BP acquired from a well-preserved piece of wood at a depth of 17 m. The dashed lines and the question marks outline that the drawn curve is arbitrary and preliminary based on current data.

(14 uncal. ka BP) depending on the location, passed below modern level at 12.6±0.2 cal. ka BP (10.6 uncal. ka BP) and decreased to −25 m below the current level around 10.6±0.1 cal. ka BP (9.4 uncal. ka BP). The lowstand have reached −30 m in southern Newfoundland (Shaw & Forbes 1995). After the lowstand, the RSL rose again from *c.* 10.2 cal. ka BP (*c.* 9 uncal. ka BP) until today (Forbes *et al.* 1993; Bell *et al.* 2003). According to Shaw *et al.* (2002), the New Brunswick and Prince Edward Island coasts were initially briefly submerged after the deglaciation. After *c.* 16 cal. ka BP (13 uncal. ka BP), the RSL decreased enough to close the Northumberland Strait by *c.* 10.2 cal. ka BP (9 uncal. ka BP). The RSL rose again from *c.* 7 cal. ka BP (6 uncal. ka BP). The same scenario occurred in northern Nova Scotia: the RSL reached +40 m after the deglaciation and then dropped to −30 m in the early Holocene (Stea 2000; Shaw *et al.* 2002).

The overall picture of the preliminary RSL variation curve for the Magdalen Islands shows some general trends (Fig. 13): (i) the southern and central part of the archipelago were deglaciated and affected by high RSL before the north; (ii) in the north, the RSL reached at least +18 m (PAL-north site); (iii) in the south, the RSL reached at least +24 m (ACW site); (iv) from *c.* 15 ka, the entire archipelago was partially submerged by a high sea level; and (v) from *c.* 10 ka, the RSL dropped drastically to reach a depth of at least ~−17 m at *c.* 9.8 ka. The RSL appears to have passed below the current sea level *c.* 10.7 ka, which is consistent with the regional literature (e.g. Shaw *et al.* 2002; Bell *et al.* 2003). Many studies described submarine relief forms testifying a maximum depth for the lowstand. Based on marine terraces mapped between −36 m (Sanschagrin 1964) and up to −62 m (Loring & Nota 1966), Dredge *et al.* (1992) suggested

a lowstand for the MIS 2 period, as they thought that the Magdalen Islands were ice-free during the MIS 2. Loring & Nota (1973), and more recently Audet-Morin (2010), mentioned that the Magdalen Shelf around the archipelago is incised by well-defined valleys (~20–200 m) interpreted to be part of a former drainage system. Audet-Morin (2010) mapped a few valleys at ~35 m depth within approximately 10 km offshore of Havre-Aubert Island. Josenhans & Lehman (1999) also reported a marine terrace at a depth of ~100 m around the Magdalen Shelf, attesting to a low sea-level event. However, the timing of the lowstand is not clear; these studies refer to a post-glacial lowstand without any further details. In light of our results, we suggest a low sea-level event after 10.8 ka.

Implications for the glacial history of eastern Canada

The data presented in this paper argue that the Magdalen Islands were glaciated during the LGM and are therefore inconsistent with the 'minimum' model supported by many of our predecessors who worked on the archipelago (e.g. Prest *et al.* 1976; Dredge *et al.* 1992). However, our data are not consistent with the 'maximum' model either. The only sedimentological evidence of the LIS on the Magdalen Islands is the fluvioglacial deposit that lies on the bedrock well under the Grande-Entrée till/stone line (PAL-north site). As the latter is dated to the LGM, the LIS fluvioglacial unit is likely to be older than MIS 2. Based on the same deposit, Dredge *et al.* (1992) proposed a pre-MIS 5 glaciation of the archi-

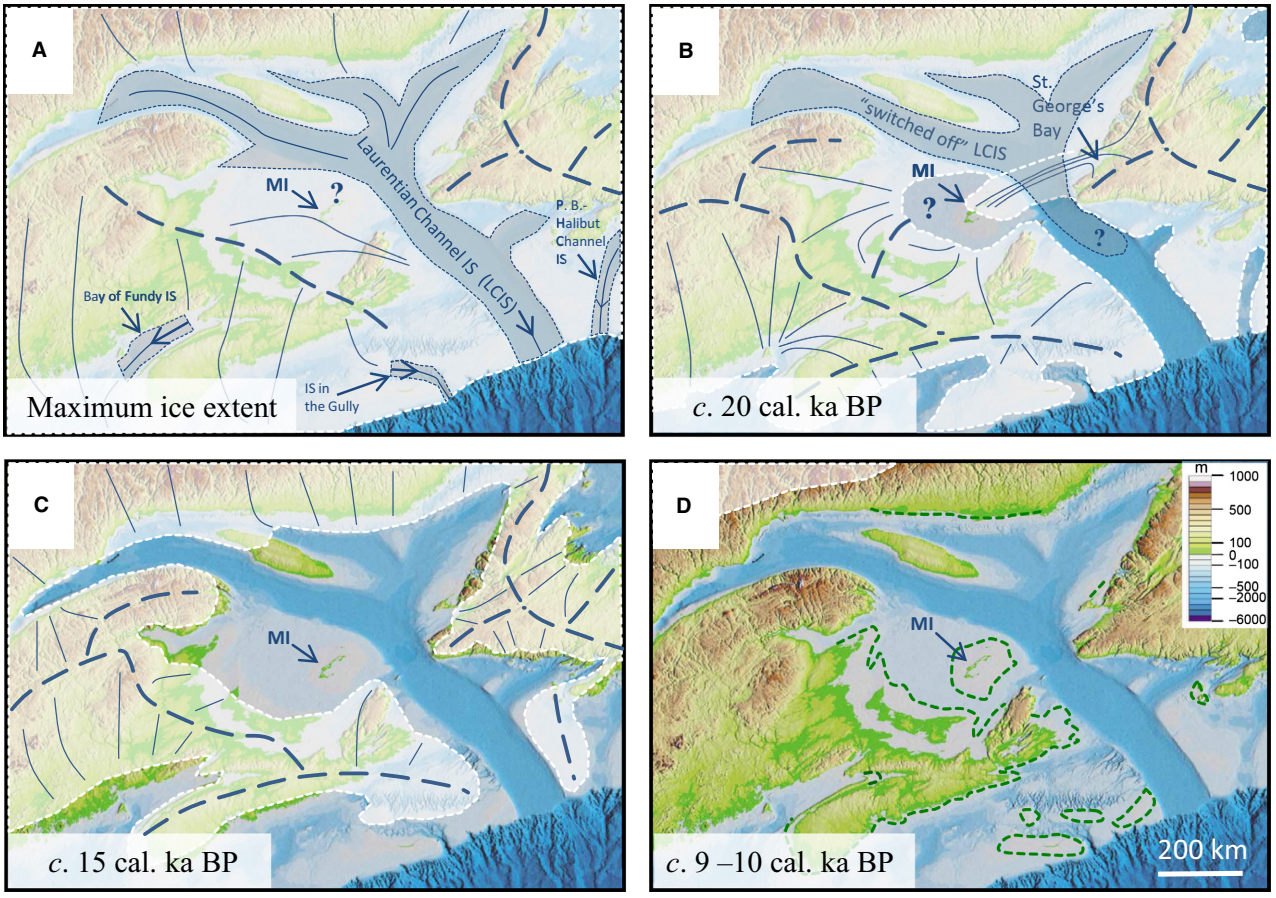

Fig. 14. Schematic representation of the main interpretations discussed in this study. The underlying digital elevation model (m a.s.l.) is a shaded relief image of the Atlantic Canada DEM used by Shaw *et al.* (2002). Heavy blue dashed lines are major ice divides, thin blue lines are generalized flowlines, and white dashed lines are approximate ice margins, all according to Shaw *et al.* (2006), but re-interpreted with the new data presented in this study. Legend and scale in D are valid for all. MI = Magdalen Islands. A. Maximum ice extent during the Last Glacial Maximum (LGM). Grey polygons with dashed outlines are major ice streams (IS) outlined by Margold *et al.* (2015). The northern archipelago is included in the global model despite there being no evidence of a glaciation by the Escuminac icecap on the northern islands (see Discussion). P.B. = Placentia Bay. B. Ice margins at *c.* 20 cal. ka BP. The southern Magdalen Islands were deglaciated and affected by a high sea level and periglacial processes. The northern archipelago was glaciated by an ice flow from Newfoundland (St George's Bay) that reached the islands while the Laurentian Channel ice stream (LCIS) was inactive (or 'switched off') (see Discussion). C. Ice margins at *c.* 15 cal. ka BP. The entire Magdalen Islands were partially submerged. D. Around 9–10 cal. ka BP, the relative sea level stood below the current level. Dark green dashed lines are land extent adapted from Shaw *et al.* (2002).

pelago by the LIS. Generally, our data fit with the Appalachian Glacier Complex (AGC) model, as two ice flows coming from two different local icecaps were identified on the archipelago and dated approximately to the LGM. By comparing our data with the regional syntheses (Stea *et al.* 1998, 2011; Josenhans & Lehman 1999; Stea 2004; Shaw *et al.* 2006; Josenhans 2007), it is clear that our data set provides significant new information for the Magdalen Islands region and thus for the central part of the Gulf of St. Lawrence. Primarily, the ice flow from the Newfoundland icecap identified on the northern part of the archipelago is novel. The AGC model, as described for example by Shaw *et al.* (2006) or Stea *et al.* (2011), argues that the LIS formed an ice stream in the Laurentian Channel during the LGM, which is in contradiction with an ice flow from Newfoundland. However, based on an extensive study of subglacial bedforms across Newfoundland, McHenry & Dunlop (2015) presented maps on which an ice flow towards the WSW from St George's Bay is highly probable. From the glaciotectonic deformation and clast fabric orientations observed on the northern archipelago, the Magdalen Islands are on the ice-flow axis of St George's Bay. McHenry & Dunlop (2015) did not present a chronology for the ice flow in St George's Bay. Nonetheless, our data indicate an age of 19.8±1.4 ka (OSL90) for the Grande-Entrée till at the Old-Harry site, suggesting a glaciation from the Newfoundland icecap at the end of the LGM. For such a scenario to occur, the Laurentian Channel, which is ~400 m deep and ~70 to 100 km wide, must have been ice-filled with an inactive ice stream for a significant period of time. Studies carried out on modern ice sheets suggest that ice streams show significant spatial and temporal variability, with some ice streams known to have switched on and off (e.g. Margold *et al.* 2015). This variability is attributed to either external forcing such as changes in atmospheric or oceanic conditions, or internal forcing (e.g. Bennett 2003). Margold *et al.* (2015) pointed out that, although a comprehensive knowledge of the spatial extent of palaeo-ice streams exists, there is a major gap in the understanding of the timing of ice-stream operation within the LIS. Notwithstanding this lack of information, we propose the hypothesis that at the end of the LGM, the Laurentian Channel ice stream (LCIS) switched off, allowing the Newfoundland icecap to reach the northern Magdalen Islands from St George's Bay and across the Laurentian Channel (Fig. 14B). This scenario might be possible if at the end of the LGM climatic or oceanic conditions changed drastically, for instance, if the LIS received much less precipitation than the Newfoundland icecap, which is quite likely owing to the closer location of the latter to the Atlantic Ocean. However, it is assumed that during the LGM climax, the LCIS was probably active (switched on), impeding ice from Newfoundland from crossing the Laurentian Channel (Fig. 14A). Another hypothesis is that when the LCIS switched off and started to melt, the stress conditions changed, buttressing removed and re-advances were triggered in this case in the Newfoundland icecap, at least through St George's Bay. This scenario was suggested by Josenhans & Lehman (1999) to explain major re-advances off Baie des Chaleurs and in the Cape Breton Channel after the retreat of the LCIS between *c.* 14.7 and 14.1 cal. ka BP (13.2 and 12.7 uncal. ka BP). Although these re-advances occurred much later, this scenario might have triggered the Newfoundland ice movement towards the Magdalen Islands. Josenhans & Lehman (1999) suggested that around 16.5 cal. ka BP (14.3 uncal. ka BP), the ice in the Laurentian Channel was at least to the north of the Cabot Strait, which was ice-free, and by *c.* 16.1 cal. ka BP (14.1 uncal. ka BP), the ice was to the north of St George's Bay, indicating that the Newfoundland lobe also retreated from the Laurentian Channel at that time. As there is no evidence of the Escuminac icecap on the northern archipelago, we hypothesize that either (i) the northern Magdalen Islands remained ice-free (as nunataks) during the LGM climax, or (ii) evidence of Escuminac glaciation was totally removed by the subsequent glaciation by the Newfoundland ice, or (iii) this part of the archipelago was affected by cold-based ice within the Escuminac icecap, leaving therefore no evidence.

The location of the Escuminac icecap in the west of the Gulf of St. Lawrence is well recognized although its ice-divide position is still discussed in the regional literature (e.g. Shaw *et al.* 2006; Stea *et al.* 2011). According to Rémillard *et al.* (2013), the Escuminac icecap would have extended approximately southeastward on the southern Magdalen Islands during the MIS 2, which is consistent with the ice divide suggested by Shaw *et al.* (2006) to the northwest of the archipelago (Fig. 14A). The deglaciation of the southern archipelago started while the north was still glaciated by the Newfoundland icecap (Fig. 14B). As soon as the southern islands were deglaciated, they were partially submerged and affected by periglacial processes (Rémillard *et al.* 2015a). Around 15 ka, the entire archipelago was ice-free and partially submerged (Fig. 14C). As discussed in the *Post-LGM sea-level variations* section, the sea level passed below modern level around 10.7 ka and reached a regional lowstand of unknown maximum depth after 10 ka (Fig. 14D).

Conclusions

In addition to the extensive chronology presented in this paper, the stratigraphical descriptions and the sedimentological analyses carried out on 21 sequences

located throughout the Magdalen Islands archipelago draw an overall picture of its palaeogeographical history from the LGM to the early Holocene. During the LGM, the islands were at the crossroads of two different icecaps; the southern islands were glaciated by the Escuminac icecap located in the western Gulf of St. Lawrence whereas at the end of the LGM, the northern archipelago was glaciated by an ice flow from Newfoundland during an inactive period of the Laurentian Channel ice stream. This scenario argues against both the 'minimum' and 'maximum' conceptual models suggested during the 20th century for the Maritime Provinces of eastern Canada. The new data are instead consistent with the Appalachian Glacier Complex (AGC) scenario and provide details for the central area of the Gulf of St. Lawrence. Our data also reveal that the southern islands were deglaciated early after the LGM and were affected by a high sea level as well as periglacial processes, while the northern archipelago was still ice-covered (*c.* 20 ka). Around 15 ka, the entire archipelago was deglaciated and partially submerged until *c.* 11 ka. The relative sea level (RSL) fell below the current sea level around 10.7 cal. ka BP. This study is the first major contribution to a detailed stratigraphical and independently validated absolute chronology of the Quaternary history of the Magdalen Islands and represents the first step towards the establishment of a complete RSL variation curve for the archipelago.

Acknowledgements. – Gabriel Ladouceur is thanked for his valuable help in the field, as well as Marie-Pier St-Onge, Jacques Labrie and Quentin Beauvais for their help in the laboratory. The authors wish to acknowledge the support of the technical staff of the Nordic Laboratory for Luminescence Dating (NLL). The Natural Sciences and Engineering Research Council of Canada (NSERC), the *Fonds de recherche du Québec Nature et Technologies* (FRQNT), the Coastal Geoscience Chair and the Canada Research Chair in Marine Geology provided financial support for the project. We also thank John Shaw and Mark Bateman for the constructive and helpful comments that greatly improved the manuscript. Comments by the Editor Jan A. Piotrowski are also much appreciated.

References

Aitken, M. J. 1985: *Thermoluminescence Dating*. 359 pp. Academic Press Inc., London.

Alcock, F. J. 1941: The Magdalen Islands, their geology and mineral deposits. *Transactions of the Canadian Institute of Mine of Metallurgy 44*, 623–649.

Anonymous. 1981: Une découverte en fonçant le puits no. 2. *L'explorateur 3*, p. 2.

Audet-Morin, M. 2010: *Géomorphologie marine des zones extracôtières est et sud des Îles-de-la-Madeleine, Québec*. M.Sc. thesis, Université Laval, 57 pp.

Barnhardt, W. A., Gehrels, W. R., Belknap, D. F. & Kelley, J. T. 1995: Late Quaternary relative sea-level change in the western Gulf of Maine: evidence for a migrating glacial forebulge. *Geology 23*, 317–320.

Bell, T., Batterson, M. J., Liverman, D. G. E. & Shaw, J. 2003: A new late-glacial sea-level record for St. George's Bay, Newfoundland. *Canadian Journal of Earth Sciences 40*, 1053–1070.

Bell, T., Daly, J., Batterson, M. J., Liverman, D. G. E., Shaw, J. & Smith, I. R. 2005: Late Quaternary relative sea-level change on the west coast of Newfoundland. *Géographie physique et Quaternaire 59*, 129–140.

Bennett, M. R. 2003: Ice streams as the arteries of an ice sheet: their mechanics, stability and significance. *Earth-Science Reviews 61*, 309–339.

Blott, S. J. & Pye, K. 2001: Gradistat: a grain size distribution and statistics package for the analysis of unconsolidated sediments. *Earth Surface Processes and Landforms 26*, 1237–1248.

Bøtter-Jensen, L., Thomsen, K. & Jain, M. 2010: Review of optically stimulated luminescence (OSL) instrumental developments for retrospective dosimetry. *Radiation Measurements 45*, 253–257.

Brisebois, D. 1981: *Lithostratigraphie des strates Permo-Carbonifères de l'archipel des Îles de la Madeleine*. 48 pp. Ministère de l'Énergie et des Ressources du Québec, Québec, DPV-796, Québec.

Buylaert, J.-P., Murray, A. S., Gebhardt, A. C., Sohbati, R., Ohlendorf, C., Thiel, C., Wastegård, S., Zolitschka, B. & The PASADO Science Team 2013: Luminescence dating of the PASADO core 5022-1D from Laguna Potrok Aike (Argentina) using IRSL signals from feldspar. *Quaternary Science Reviews 71*, 70–80.

Carr, S. J. & Rose, J. 2003: Till fabric patterns and significance: particle response to subglacial stress. *Quaternary Science Reviews 22*, 1415–1426.

Chalmers, R. 1895: Report on the surface geology of southern New Brunswick, north-western Nova Scotia and a portion of Prince Edward Island. *Geological Survey of Canada, Annual Report*, 144 pp.

Clarke, J. M. 1911: Observations on the Magdalen Islands. *New York State Museum Bulletin 149*, 134–156.

Coleman, A. P. 1919: The glacial history of Prince Edward Island and the Magdalen Islands. *Proceedings and Transactions of the Royal Society of Canada 13*, 33–37.

Cunningham, A. C. & Wallinga, J. 2010: Selection of integration time intervals for quartz OSL decay curves. *Quaternary Geochronology 5*, 657–666.

Dredge, L. A. & Grant, D. R. 1987: Glacial deformation of bedrock and sediment, Magdalen Islands and Nova Scotia, Canada: evidence for a regional grounded ice sheet. *In* van der Meer, J. J. M. (ed.): *Tills and Glaciotectonics: Proceedings of an INQUA Symposium on Genesis and Lithology of Glacial Deposits*, 183–195. Balkema, Rotterdam.

Dredge, L. A., Mott, R. J. & Grant, D. R. 1992: Quaternary stratigraphy, paleoecology, and glacial geology, Iles de la Madeleine, Québec. *Canadian Journal of Earth Science 29*, 1981–1996.

Duller, G. A. T. 2003: Distinguishing quartz and feldspar in single grain luminescence measurements. *Radiation Measurements 37*, 161–165.

Dyke, A. S. & Peltier, W. R. 2000: Forms, response times and variability of relative sea-level curves, glaciated North America. *Geomorphology 32*, 315–333.

Dyke, A. S. & Prest, V. K. 1987: Late Wisconsinan and Holocene history of the Laurentide Ice Sheet. *Géographie Physique et Quaternaire 41*, 237–263.

Dyke, A. S., Andrews, J. T., Clark, P. U., England, J. H., Miller, G. H., Shaw, J. & Veillette, J. J. 2002: The Laurentide and Innuitian ice sheets during the last glacial maximum. *Quaternary Science Reviews 21*, 9–31.

Evans, D. J. A., Phillips, E. R., Hiemstra, J. F. & Auton, C. A. 2006: Subglacial till: formation, sedimentary characteristics and classification. *Earth-Sciences Reviews 78*, 115–176.

Folk, R. L. & Ward, W. C. 1957: Brazos River bar: a study in the significance of grain size parameters. *Journal of Sedimentary Petrology 27*, 3–26.

Forbes, D. L., Shaw, J. & Eddy, B. G. 1993: Late Quaternary sedimentation and the postglacial sea-level minimum in Port-au-Port Bay and vicinity, west Newfoundland. *Atlantic Geology 29*, 1–26.

Fuchs, M. & Owen, L. A. 2008: Luminescence dating of glacial and associated sediments: review, recommendations and future directions. *Boreas 37*, 636–659.

Giles, P. S. 2008: Windsor Group (Late Mississippian) stratigraphy, Magdalen Islands, Quebec: a rare eastern Canadian record of late Visean basaltic volcanism. *Atlantic Geology 144*, 167–185.

Godfrey-Smith, D. L., Huntley, D. J. & Chen, W. H. 1988: Optically dating studies of quartz and feldspar sediment extracts. *Quaternary Science Reviews 7*, 373–380.

Goldthwait, J. W. 1915: The occurrence of glacial drift on the Magdalen Islands. *Canada Geological Survey, Department of Mines, Museum Bulletin 14, Geological Series 25*, 11 pp.

Grant, D. R. 1989: Le Quaternaire de la région des Appalaches atlantiques du Canada. *In* Fulton, R. J. (ed.): *Le Quaternaire du Canada et du Groenland, Géologie du Canada*, 412–474. Geological Survey of Canada, Ottawa.

Guérin, G., Mercier, N. & Adamiec, C. 2011: Dose-rate conversion factors: update. *Ancient TL 29*, 5–8.

Hamelin, L.-E. 1959: *Sables et mer aux Îles de la Madeleine*. 75 pp. Ministère de l'Industrie et du Commerce, Québec.

Hansen, V., Murray, A. S., Buylaert, J.-P., Yeo, E. Y. & Thomsen, K. J. 2015: A new irradiated quartz for beta source calibration. *Radiation Measurements 81*, 123–127.

Josenhans, H. 2007: Atlas of the marine environment and seabed geology of the Gulf of St. Lawrence. *Geological Survey of Canada, File 5346*, 142 pp.

Josenhans, H. & Lehman, S. 1999: Late glacial stratigraphy and history of the Gulf of St. Lawrence, Canada. *Canadian Journal of Earth Sciences 36*, 1327–1345.

Kelley, A. R., Kelley, J. T., Belknap, D. F. & Gontz, A. M. 2011: Coastal and terrestrial impact of the isostatically forced Late Quaternary drainage divide shift, Penobscot and Kennebec Rivers, Maine, USA. *Journal of Coastal Research 27*, 1085–1093.

Laverdière, C. & Guimont, P. 1974: Un froid à sol fendre. *Geos 2*, 18–20.

Loring, D. & Nota, D. 1966: Sea-floor conditions around the Magdalen Islands in the southern Gulf of St. Lawrence. *Journal of the Fisheries Research Board of Canada 23*, 1197–1207.

Loring, D. & Nota, D. 1973: Morphology and sediments of the Gulf of St. Lawrence. *Service des pêches et des sciences de la mer, Bulletin 182*, 147 pp.

Margold, M., Stokes, C. R. & Clark, C. D. 2015: Ice stream in the Laurentide Ice Sheet: identification, characteristics and comparison to modern ice sheets. *Earth-Science Reviews 143*, 117–146.

Mark, D. M. 1973: Analysis of axial orientation data including till fabrics. Geological Society of America Bulletin 84, 1369–1374.

McHenry, M. & Dunlop, P. 2015: The subglacial imprint of the last Newfoundland Ice Sheet, Canada. *Journal of Maps 22 pp*. doi: 10.1080/17445647.2015.1044038.

Murray, A. S. & Wintle, A. G. 2000: Luminescence dating of quartz using an improved single-aliquot regenerative-dose protocol. *Radiation Measurement 32*, 57–73.

Murray, A. S. & Wintle, A. G. 2003: The single aliquot regenerative dose protocol: potential for improvements in reliability. *Radiation Measurement 37*, 377–381.

Murray, A. S., Marten, R., Johnston, A. & Martin, P. 1987: Analysis for naturally occurring radionuclides at environmental concentrations by gamma spectrometry. *Journal of Radioanalytical and Nuclear Chemistry 115*, 263–288.

Murray, A. S., Thomsen, K. J., Masuda, N., Buylaert, J.-P. & Jain, M. 2012: Identifying well-bleached quartz using the different bleaching rates of quartz and feldspar luminescence signals. *Radiation Measurements 47*, 688–695.

Paquet, G. 1989: *L'évolution de la plate-forme gréseuse de l'Île du Cap-aux-Meules (Îles-de-la-Madeleine, Québec)*. M.Sc. thesis, Université de Montréal, 223 pp.

Parent, P. & Dubois, J.-M. M. 1988: Stratigraphie et événements du Quaternaire, Îles-de-la-Madeleine, Québec. – Indices de centres de dispersion glaciaire sur le plateau madeleinien. *In* Hétu, B. (ed.): *Proceedings, 6e Congrès de l'Association québécoise pour l'étude du Quaternaire*, Rimouski.

Prescott, J. R. & Hutton, J. T. 1994: Cosmic ray contributions to dose rates for luminescence and ESR dating: large depths and long-term time variations. *Radiation Measurements 23*, 497–500.

Prest, V. K., Terasme, J., Matthews, J. V. & Litchti-Federovich, S. 1976: Late-Quaternary Magdalen Islands, Quebec. *Maritime Sediments 12*, 39–59.

Quinlan, G. & Beaumont, C. 1981: A comparison of observed and theoretical postglacial relative sea level in Atlantic Canada. *Canadian Journal of Earth Sciences 18*, 1146–1163.

Reimer, P. J., Bard, E., Bayliss, A., Beck, J. W., Blackwell, P. G., Ramsey, C. B., Buck, C. E., Cheng, H., Edwards, R. L., Friedrich, M., Grootes, P. M., Guilderson, T. P., Haflidason, H., Hajdas, I., Hatte, C., Heaton, T. J., Hoffmann, D. L., Hogg, A. G., Hughen, K. A., Kaiser, K. F., Kromer, B., Manning, S. W., Niu, M., Reimer, R. W., Richards, D. A., Scott, E. M., Southon, J. R., Staff, R. A., Turney, C. S. M. & van der Plicht, J. 2013: INTCAL13 and MARINE13 radiocarbon age calibration curves 0–50,000 years cal BP. *Radiocarbon 55*, 1869–1887.

Rémillard, A. M., Buylaert, J.-P., Murray, A. S., St-Onge, G., Bernatchez, P. & Hétu, B. 2015b: Quartz OSL dating of late Holocene beach ridges from the Magdalen Islands (Quebec, Canada). *Quaternary Geochronology 30*, 264–269.

Rémillard, A. M., Hétu, B., Bernatchez, P. & Bertran, P. 2013: The Drift des Demoiselles on the southern Magdalen Islands (Quebec, Canada): sedimentological and micromorphological evidence of a glacial diamict of Late Wisconsinan. *Canadian Journal of Earth Sciences 50*, 545–563.

Rémillard, A. M., Hétu, B., Bernatchez, P., Buylaert, J.-P., Murray, A. S., St-Onge, G. & Geach, M. 2015a: Chronology and palaeoenvironmental implications of the ice-wedge pseudomorphs and composite-wedge casts on the Magdalen Islands (eastern Canada). *Boreas 44*, 658–675.

Richardson, J. 1881: Report of a geological exploration of the Magdalen Islands. *Geological Survey of Canada, Report of Progress 1879–1880, part VIII*, 16 pp.

Sanschagrin, R. 1964: Magdalen Islands. Ministère de l'Énergie et Ressources du Québec. *Geological Report 106*, 57 pp.

Shaw, J. & Forbes, D. L. 1995: The postglacial relative sea-level lowstand in Newfoundland. *Canadian Journal of Earth Sciences 32*, 1308–1330.

Shaw, J., Gareau, P. & Courtney, R. C. 2002: Palaeogeography of Atlantic Canada 13–0 kyr. *Quaternary Science Reviews 21*, 1861–1878.

Shaw, J., Piper, D. J. W., Fader, G. B. J., King, E. L., Todd, B. J., Bell, T., Batterson, M. J. & Liverman, D. G. E. 2006: A conceptual model of the deglaciation of Atlantic Canada. *Quaternary Science Reviews 25*, 2059–2081.

Stea, R. R. 2000: *Virtual Field Trip web site*. Nova Scotia Natural Resources, Mines and Energy Branch.

Stea, R. R. 2004: The Appalachian glacier complex in Maritime Canada. *In* Ehlers, J. & Gibbard, P. L. (eds.): *Quaternary Glaciations - Extent and Chronology, Part II: North America*, 213–232. Elsevier, New York.

Stea, R. R., Boyd, R., Fader, G. B. J., Courtney, R. C., Scott, D. B. & Pecore, S. S. 1994: Morphology and seismic stratigraphy of the inner continental shelf off Nova Scotia, Canada: evidence for a −65 m lowstand between 11,650 and 11,250 C^{14} yr B.P. *Marine Geology 117*, 135–154.

Stea, R. R., Piper, D. J. W., Fader, G. B. J. & Boyd, R. 1998: Wisconsinian glacial and sea-level history of Maritime Canada and the adjacent continental shelf: a correlation of land and sea events. *Geological Society of America Bulletin 110*, 821–845.

Stea, R. R., Seaman, A. A., Pronk, T., Parkhill, M. A., Allard, S. & Utting, D. 2011: The Appalachian Glacier Complex in Maritime Canada. *In* Ehlers, J. & Gibbard, P. L. (eds.): *Quaternary Glaciations - Extent and Chronology, Part II: North America*, 631–659. Elsevier, New York.

Thomsen, K., Murray, A. S., Jain, M. & Bøtter-Jensen, L. 2008: Laboratory fading rates of various luminescence signals from feldspar-rich sediment extracts. *Radiation Measurements 43*, 1474–1486.

Vandenberghe, J. & Czudek, C. 2008: Pleistocene cryopediments on variable terrain. *Permafrost and Periglacial Processes 19*, 71–83.

Vigneault, B. 2012: *Cadre lithostratigraphique quaternaire du nord des Îles-de-la-Madeleine*. M.Sc. thesis, Université du Québec à Rimouski, 109 pp.

Webster, I. T., Hancock, G. J. & Murray, A. S. 1995: Modelling the effect of salinity on radium desorption from sediments. *Geochimica et Cosmochimica Acta 59*, 2469–2476.

Wintle, A. G. & Murray, A. S. 2006: A review of quartz optically stimulated luminescence characteristics and their relevance in single-aliquot regeneration dating protocols. *Radiation Measurements 41*, 369–391.

Supporting Information

Additional Supporting Information may be found in the online version of this article at http://www.boreas.dk.

Fig. S1. Feldspars luminescence characteristics.

Fig. S2. Quartz OSL, feldspar IR_{50} and $pIRIR_{150}$ bleaching curves for a sample collected in a former sandy beach.

Fig. S3. $pIRIR_{150}$ ages plotted against IR_{50} ages and quartz ages, and IR_{50} ages plotted against quartz ages.

Table S1. Particle size data from this study.

Table S2. Radionuclide concentrations, water content and total dose rates of all the samples.

Table S3. Sample equivalent doses (De) and resulting IRSL ages.

Appendix S1. Completeness of bleaching using differential bleaching of quartz and K-feldspars.